2023-09-12

Influence of Microarchitecture on the Mechanical Fatigue Behaviour of Equine Subchondral Bone

Koshyk, Andrew

UNIVERSITY OF CALGARY

Influence of Microarchitecture on the Mechanical Fatigue Behaviour of Equine Subchondral Bone

by

Andrew Koshyk

A THESIS

SUBMITTED TO THE FACULTY OF GRADUATE STUDIES

IN PARTIAL FULFILMENT OF THE REQUIREMENTS FOR THE

DEGREE OF MASTER OF SCIENCE

GRADUATE PROGRAM IN BIOMEDICAL ENGINEERING

CALGARY, ALBERTA

SEPTEMBER, 2023

Abstract

Fractures of the equine metacarpophalangeal (MCP) joint are among the most common and fatal injuries experienced by racehorses. These bone injuries are a direct result of repetitive, high intensity loading of the skeleton during racing and training and there is consensus that they represent a mechanical fatigue phenomenon. Existing work has found the fatigue life of bone to be strongly determined by bone microarchitecture and the resulting stressed volume (i.e., the volume of bone stressed above yield). The purpose of this study was to quantify the influence of bone microarchitecture on the mechanical fatigue behaviour of equine subchondral bone from the MCP joint. Forty-eight subchondral bone samples were prepared from the third metacarpal (MC3) and proximal phalanx (P1) and subsequently imaged using high resolution micro-computed tomography (μCT) to quantify microarchitectural features of interest, including bone volume fraction, tissue mineral density, pore size, pore spacing, and pore number. Samples were cyclically loaded in compression to a stress of 70 MPa, and fatigue life was defined as the number of cycles until failure. Finite element models were created from the μCT images and used to quantify the stressed volume. Based on the expected log point-wise predictive density (ELPD), stressed volume was a strong predictor of fatigue life in both the MC3 and P1. Normalized stress (i.e., initial nominal strain) was also a strong predictor of fatigue life in samples from the MC3, but not for samples from the P1. This disparity can be attributed to differences in microstructure homogeneity. A regional analysis indicated fatigue life was more strongly associated with bone volume fraction in the superficial ($r^2 = 0.32$, $p < 0.001$) and middle ($r^2 = 0.70$, $p < 0.001$) regions of the subchondral bone, indicating that the cortical plate plays a more prominent role in the fatigue resistance of subchondral bone. By improving our understanding of the variance in fatigue life measurements, this research helps begin to clarify the underlying mechanisms of the mechanical fatigue process and provide a basic understanding of subchondral bone injuries in the equine fetlock joint.

Preface

Chapter 3 of this thesis is based on:

Koshyk, A., Pohl, A.J., Takahashi, Y., Scott, W.M., Sparks, H.D., Edwards, W.B. (2023). Mechanical fatigue behaviour of equine subchondral bone from the third metacarpal and proximal phalanx. *In preparation for submission to Bone.*

Statement of contributions: AK and WBE conceived the study design. AK preformed the experimental testing, data analysis and wrote the manuscript with input from all authors. AJP preformed the statistical analysis. YT and WMS provided critical feedback. HDS facilitated specimen collection and provided critical feedback. WBE supervised the research, provided critical feedback and helped interpret the results.

This research was approved by the University of Calgary institutional ethics board through a "Statement of Animal Tissue or Cadaver Use" protocol (Ethics ID: #AC20-0152).

Acknowledgements

I would like to acknowledge several individuals who contributed to various aspects of my graduate degree. First and foremost, I would like to thank Dr. Brent Edwards. I truly cannot express enough how grateful I am for the opportunity you gave me to join the lab. I am so appreciative of the guidance and support you have offered me over the last two years, and I really cannot imagine studying anywhere else.

I would also like to thank my supervisory committee, Dr. Sarah Manske and Dr. Michael Scott, for their guidance and feedback throughout the project. I would also like to thank Dr. Holly Sparks for all of her amazing help throughout my degree and Dr. Yuji Takahashi for his help and input on the project. I would also like to thank Dr. Brent Lievers for taking part in my defence.

To the lab group, thank you for making the lab such a wonderful environment to be in. I would like to give special thanks to Andy Pohl for all of his help with statistical analysis, Andrew Sawatsky for his technical support in the lab, and Dr. Ifaz Haider for his incredible patience and for always offering help whenever I needed it. To my friends and officemates in the HPL, thank you for making the HPL such a great place. I cannot imagine a better and more enjoyable place to work, and I will never forget the amazing friendships, laughs, and connections I built during my time here.

Finally, I would like to thank my family. I cannot begin to describe how much I appreciate your support. I always look forward to our group phone calls as a source of encouragement and entertainment. I can always count on you to help me through difficult times, make me laugh, and help me remember what is important. I could not have done this without you.

Table of Contents

List of Tables

List of Figures

List of Symbols, Abbreviations, and Nomenclature

BVF	Bone volume fraction
DEA	Discrete element analysis
E	Elastic modulus
E*	Initial elastic modulus
ELPD	Expected log point-wise predictive density
FEA	Finite element analysis
GPa	Gigapascal
HR-pQCT	High-resolution peripheral quantitative computed tomography
Hz	Hertz
IGFA	Image guided failure assessment
kg	Kilogram
kN	Kilonewton
kVp	Kilovoltage peak
MC3	Third metacarpal
MCP	Metacarpophalangeal
mm	Millimetre
MPa	Megapascal
ms	Millisecond
N	Newton
N_f	Fatigue life (Number of cycles to failure)
P1	Proximal phalanx
PBS	Phosphate buffered saline
RMSE	Root mean squared error
SD	Standard deviation
STL	Stereolithography
SV	Stressed volume (volume of material stressed above yield)
TMD	Tissue mineral density
µA	Microamps
µCT	Micro computed tomography
µm	Micrometre
σ	Stress
σ/E*	Normalized stress (analogous to initial strain)

Chapter One

Introduction

1.1 Rationale

Musculoskeletal injuries are a significant source of lost training time and morbidity among racehorses. Bone injuries account for the largest proportion of fatalities among equine athletes, particularly at the metacarpophalangeal (MCP) joint, where fractures of the third metacarpal (MC3) and proximal phalanx (P1) account for the majority of these catastrophic bone injures (Johnson et al., 1994; Rosanowski et al., 2017, 2019). Fractures of the MCP joint initiate in the subchondral bone and occur in horses that habitually race and train at high speeds. Additionally, these injuries appear to precede any associated fall or traumatic event and display a highly consistent pathological morphology, as the fractures typically originate at similar locations and propagate along similar lines (Riggs, 1999). Therefore, there is consensus that these injuries represent a mechanical fatigue phenomenon (Colgate & Marr, 2020; Martig et al., 2014; Riggs, 1999, 2002; Riggs et al., 1999a).

Mechanical fatigue is characterized by the accumulation of microdamage as a result of repetitive, cyclic loading (Suresh, 1998). Over time, this accumulation of microdamage diminishes the quality of the bone in the form of decreased stiffness and strength (Burr et al., 1998; Carter & Hayes, 1977). In the absence of adequate repair and remodelling, the accumulation of microdamage may eventually lead to failure at loads well below the monotonic ultimate strength of the material. While the fatigue behaviour of equine subchondral bone has been previously described (Martig et al., 2013), mechanical fatigue is a stochastic process and exhibits a considerable amount of variation. Existing work has found the fatigue life of bone to be strongly

determined by bone microarchitecture and the resulting stressed volume (i.e., the volume of bone stressed above yield) (Carter et al., 1981a; Fatihhi et al., 2015; Loundagin et al., 2021; Loundagin & Edwards, 2020; Rapillard et al., 2006; Topoliński & Mazurkiewicz, 2012; Zioupos et al., 2008). In equine subchondral bone, Martig et al. (2020) determined that compressive fatigue life was associated with apparent stiffness and bone volume fraction. However, beyond our understanding of the importance of bone volume fracture, a mechanistic understanding of the relationship between bone quality and fatigue resistance is lacking, which significantly limits our ability to predict fatigue failure.

1.2 Objective and Hypothesis

The objective of this work is to quantify the influence of microarchitecture on the fatigue behaviour of equine subchondral bone. This will be accomplished through a combination of high-resolution imaging, biomechanical testing, and finite element modelling. Our primary aim is to determine if stressed volume can predict fatigue life better than normalized stress (i.e., initial nominal strain). Our secondary aim is to establish the relationship between stressed volume and microarchitecture at different regions throughout subchondral bone from the MCP joint. We hypothesize that stressed volume will predict fatigue life better than normalized stress and that a higher stressed volume will be associated with lower bone volume fraction.

1.3 Presentation of the Thesis

The content of this thesis is organized as follows. Chapter Two summarizes the relevant literature and background information, including the aetiopathogenesis of MCP joint injuries, mechanical fatigue of cortical and trabecular bone, and the influence of microarchitecture on the mechanical properties of bone. Chapter Three addresses the objectives and specific aims outlined

in section 1.2 of this thesis. This chapter is written as an independent manuscript. Chapter Four synthesizes the findings of the study, discusses the strengths and limitations, and considers the implications and future directions of this research.

Chapter Two

Background

2.1 Fractures of the Metacarpophalangeal Joint

Musculoskeletal injuries are a significant source of lost training time and morbidity in racehorses. Bone injuries account for the majority of fatalities among equine athletes (77%), particularly at the metacarpophalangeal (MCP) joint, where fractures of the third metacarpal (MC3) and proximal phalanx (P1) account for the largest proportion (51%) of these catastrophic bone injuries (Johnson et al., 1994; Rosanowski et al., 2017).

The MCP joint is comprised of the MC3, the P1, and the sesamoid bones (Figure 2-1). During locomotion, the MCP joint undergoes a significant amount of flexion that helps store a large amount of elastic strain energy in the soft tissue, namely the tendons and ligaments. This stored energy assists in reducing the work of galloping racehorses, as the passive energy return aids in limb advancement and forward motion (Santschi, 2008). However, while this flexion assists in efficient locomotion by storing elastic strain energy, it also puts the joint at high risk of injury, as tendon wrapping at this location generates extremely high cyclic loads. Existing work has estimated contact forces between the MC3 and P1 to reach almost 25,000 N for a 500 kg horse when galloping (Harrison et al., 2010).

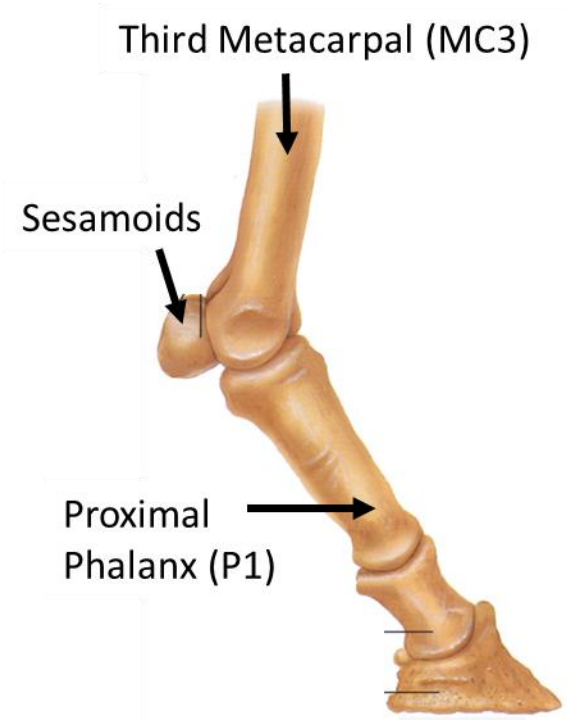

Figure 2-1: Skeletal anatomy of the fetlock joint (Riegel & Hakola, 1996)

Injuries at the MCP joint initiate in the subchondral bone, which refers to the bone underlying the calcified cartilage, including both the subchondral cortical plate and subchondral trabecular bone. In the MC3, condylar fractures often develop in the palmar aspect of the joint and are typically parasagittal, involving the groove between the medial or lateral condyle and the sagittal ridge on the distal end of the MC3 (Radtke et al., 2003; Riggs, 1999; Riggs et al., 1999a). Lateral condylar fractures of the MC3 initially propagate along the sagittal plane before curving abaxially, eventually exiting through the lateral cortex, whereas medial condylar fractures propagate proximally along the sagittal plane and typically spiral along the diaphysis (Ellis, 1994). Fractures of the P1 often occur along the sagittal plane and propagate distally from the mid-sagittal groove of the proximal joint surface (Nixon, 2020) (Figure 2-2).

Figure 2-2: Radiograph of a (A) lateral condylar fracture, (B) medial condylar fracture, and (C) fracture of the P1 (Riggs, 1999)

Fractures of the MCP joint typically occur in horses that habitually perform at high speeds and appear to precede any associated fall or traumatic event. Furthermore, these fractures have a predictable configuration and pre-existing microcracks, similar to the fatigue damage detected from experimental testing, are observed in the subchondral bone at the sites of intra-articular fractures (Ellis, 1994; Stepnik et al., 2004). Therefore, there is a consensus that these bone injuries in racehorses are a direct result of repetitive high intensity loading of the skeleton and, consequently, are considered a mechanical fatigue injury (Colgate & Marr, 2020; Martig et al., 2014; Riggs, 1999; Riggs et al., 1999a).

2.2 Mechanical Fatigue

Mechanical fatigue is characterized by the accumulation of microdamage in a material subjected to repetitive, cyclic loading (Suresh, 1998). This microdamage leads to a progressive

degradation in material properties and the eventual failure at loading magnitudes well below the monotonic ultimate strength (Burr et al., 1990; Carter & Hayes, 1977). The phenomenon of fatigue failure is not limited to engineering materials, but also manifests in biological materials subjected to repetitive loading and cumulative bouts of activity, such as in the MCP joint of equine athletes.

The mechanical fatigue behaviour of bone has been well described through *ex vivo* cadaveric testing. Several studies have explored the relationship between the fatigue life of bone and a variety of loading parameters, including loading magnitude, frequency, and mode, by cyclically loading small bone samples (Caler & Carter, 1989; Carter & Hayes, 1976; Martig et al., 2013; Rapillard et al., 2006; Zioupos et al., 2001). The fatigue behaviour is typically represented using a stress-life curve, which plots the stress amplitude on the vertical axis and the fatigue life, defined as the number of loading cycles a material can withstand before failure, on the horizontal axis (Figure 2-3). The fatigue life is often plotted using a logarithmic scale, meaning that for small changes in the applied stress, there can be disproportionately large changes in the resulting fatigue life. When plotted, the fatigue life data is typically well described with an inverse power curve. However, owing to the inherent variability in bone tissue, there exists a significant amount of scatter in the data, often spanning multiple orders of magnitude (Carter et al., 1981a; Taylor et al., 1999). This variability is seen despite holding all extrinsic loading parameters constant, suggesting that it is not a result of the experimental setup. Instead, Taylor (1998) proposed that the variance may be explained by the concept of stressed volume. Since failure will initiate at the weakest region within a sample, a larger sample is statistically more likely to contain a critical flaw. This concept was able to accurately predict scatter within fatigue life data (Taylor et al., 1999). Together, these findings suggest that the observed scatter in fatigue life data can be attributed to inherent differences in bone microarchitecture.

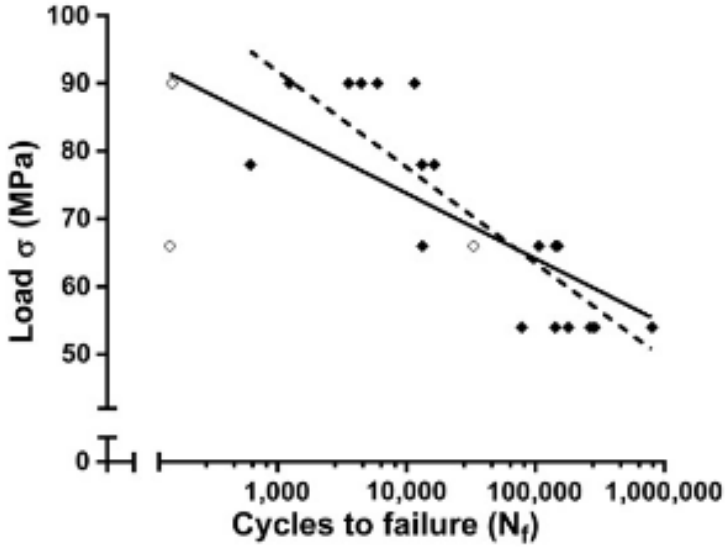

Figure 2-3: Stress-life plot of subchondral bone taken from the equine third metacarpal (Martig et al., 2013)

2.3 Bone Structure

Bone is a hierarchical structure with varying length scales and levels of organization all working in conjunction to carry out mechanical and biological functions. In the MCP joint, injuries develop in the subchondral bone, which refers to the bone tissue underlying the calcified cartilage and includes both the subchondral cortical plate and subchondral trabecular bone (Figure 2-4). The subchondral bone plate is a thin layer of cortical bone responsible for providing mechanical strength to support the overlying articular cartilage. Underneath the cortical bone plate lies the subchondral trabecular bone, which is more metabolically active compared to the cortical bone (Zhu et al., 2021). The function of the subchondral bone is to attenuate forces at the joint, with the subchondral cortical plate providing firm support and the subchondral trabecular bone providing elasticity for shock absorption (McIlwraith et al., 2015).

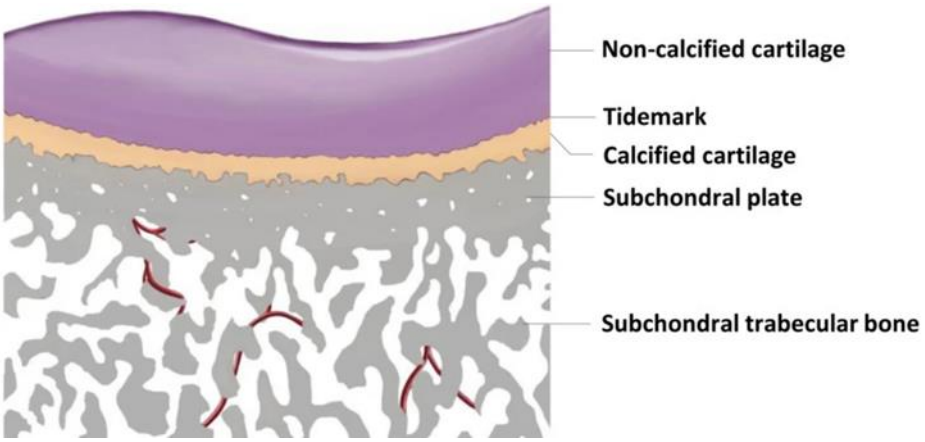

Figure 2-4: Structure of subchondral bone (Li et al., 2013)

Cortical bone can be examined at multiple length scales (Figure 2-5). At the nanostructural scale, the organic matrix, composed primarily of collagen fibres, is surrounded and infiltrated by a mineral phase. The organic collagen component is responsible for preserving toughness by contributing to bone's ability to plastically deform and absorb energy (Wang et al., 2001). While the mineral phase provides bone with its characteristic strength and rigidity, increased mineralization is also associated with reduced toughness, as it has been shown to produce a more brittle material (Currey, 2004; Currey et al., 1996). At the microstructural scale, these mineralized collagen fibres form into planar arrangements called lamellae, each approximately 5 μm thick (Ethier & Simmons, 2007). These lamellar sheets of alternating collagen fibre orientation wrap in concentric layers around a central canal to form an osteon. Osteons are approximately cylindrical, measuring about 200 μm in diameter, and run roughly parallel to the long axis of the bone, making it highly anisotropic (Ethier & Simmons, 2007). The space between osteons is referred to as interstitial bone, and the junction between an osteon and interstitial bone is known as the cement line, a highly mineralized, collagen-free layer less than 1 μm thick (Ethier & Simmons, 2007).

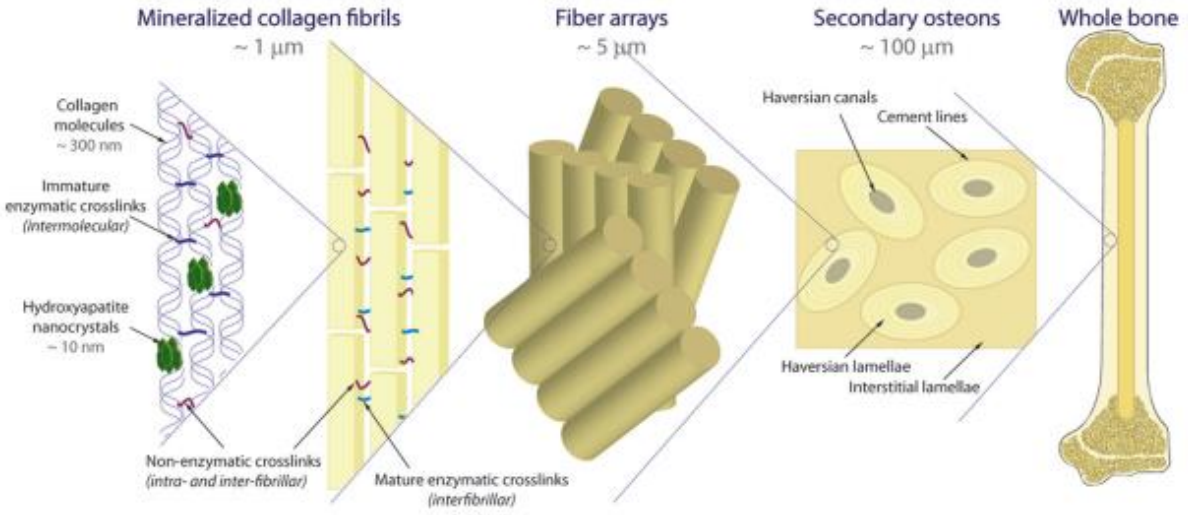

Figure 2-5: Structure of cortical bone at multiple length scales (Zimmermann & Ritchie, 2015)

Trabecular bone is comprised of a network of interconnected struts called trabeculae, which are approximately 200 μm thick in healthy bone (Ethier & Simmons, 2007). The space between adjacent trabeculae is filled with bone marrow. Like cortical bone, trabecular tissue has a lamellar structure, with lamellae running parallel to the trabeculae (Ethier & Simmons, 2007). The trabecular microstructure is typically oriented such that there is a direction along which mechanical stiffness and strength are greatest, resulting in a highly anisotropic structure (Keaveny et al., 2001). During loading, the progressive collapse of the trabecular network allows trabecular bone to undergo large compressive strains at approximately constant stress, so that large amounts of energy can be absorbed without high stresses being generated (Ethier & Simmons, 2007). Consequently, trabecular bone provides high energy absorption with minimal density and weight.

As previously mentioned, bone accumulates microdamage in response to cumulative bouts of activity. In normal, healthy bone, this microdamage is repaired by bone cells. In fact, it has been

suggested that microdamage may be required to initiate remodelling and normal turnover of the skeleton (Burr et al., 1985; Mori & Burr, 1993). Previous work determined that racehorses do indeed adapt to race training, as subchondral bone in the MCP joint of active racehorses often exhibits increased density (Easton & Kawcak, 2007; Riggs et al., 1999b; Riggs & Boyde, 1999) (Figure 2-6). However, other work has shown that intense training in equine athletes suppresses remodelling of third metacarpal subchondral bone (Holmes et al., 2014; Whitton et al., 2010), suggesting that periods of reduced loading are important for facilitating repair.

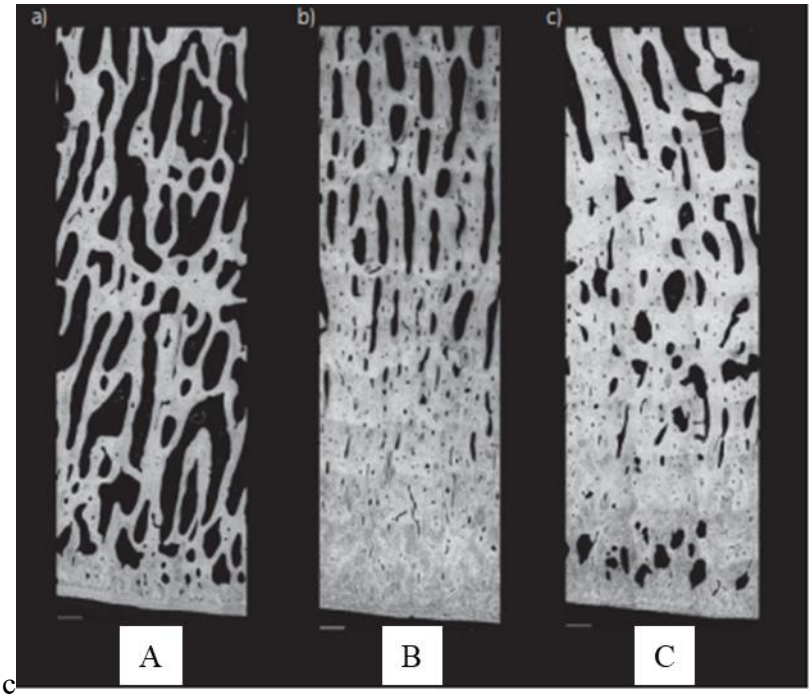

Figure 2-6: Back-scattered electron microscopy images of subchondral bone from the MC3 in Thoroughbred racehorses. The articular surface is oriented to the bottom of the figure. Samples were taken from (A) an unraced 2-year-old horse, (B) a mature horse in race training, and (C) a mature racehorse that has been resting from training for 9 weeks. (Martig et al., 2014)

2.4 Influence of Microarchitecture on the Mechanical Fatigue Behaviour of Bone

In cortical bone, the microstructural features and discontinuities within the material give rise to stress concentration sites that may lead to the initiation and propagation of microcracks. Indeed, existing work has demonstrated that local strains within the bone matrix may be considerably higher than applied nominal strains. Previous work using finite element modelling found local strains surrounding osteocyte lacunae to be more than 8 times higher than the applied strain (Verbruggen et al., 2012), while other work using digital image correlation found local strains to be as much as 15 times greater than the applied bulk strain (Nicolella et al., 2005). In addition to osteocyte lacunae, Haversian canals also give rise to stress concentrations within the bone matrix. Existing work has demonstrated that strain can be amplified by 2.4 – 2.8 times in regions adjacent to Haversian and Volkmann canals (Mullins et al., 2007; Vaughan et al., 2013). Furthermore, resorption canals formed during the remodelling process are considerably larger than Haversian canals, ranging from 200 – 300 μm in diameter (Bell et al., 1999; Cooper et al., 2016; Jordan et al., 2000). Consequently, these resorption canals drastically increase local porosity and induce large stress concentrations. Therefore, the increased strains surrounding microstructural features including Haversian canals and osteocyte lacunae may facilitate the initiation and propagation of microcracks. The stress concentrations surrounding these microstructural features are often quantified using a stress concentration factor, defined as the ratio of maximum stress to nominal stress. However, the stress concentration factor is somewhat limited in that it only quantifies the peak magnitude of the stress concentration without accounting for other aspects of the stress distribution, such as the amount of material subjected to elevated stress. To predict failure resulting from a stress concentration, it is not only necessary to know the magnitude of the stress concentration, but also the volume of material subjected to this elevated stress, as this dictates the

ability of a crack to propagate within the bony matrix. The theory of critical distances (TCD) predicts material failure will occur when the stress reaches some critical value at a critical distance from a stress concentration feature (Taylor, 1999, 2005, 2008). Similar to the TCD approach, the total stressed volume (i.e., the volume of bone stressed above yield) quantifies the stress field surrounding a stress concentration feature and may be a more practical measure for complex geometries.

While microstructural features within cortical bone give rise to stress concentration sites, these discontinuities within the material also serve as barriers to crack growth that may help bone withstand repetitive loading. Extrinsic toughening mechanisms reduce the force experienced at the crack tip and aid in resisting crack growth at the microstructural scale through the presence of osteonal structures (Launey et al., 2010; Zimmermann & Ritchie, 2015). In human cortical bone, crack deflections and twists allow for significant toughening to be generated. These deflections and twists result in a lower local driving force at the crack tip. Consequently, higher applied stresses will be required to propagate the crack further (Zimmermann & Ritchie, 2015). Crack deflections and twists often result from interactions with osteons, as osteonal cement lines provide a weak propagation path for cracks (Yeni & Norman, 2000). Therefore, extrinsic toughening mechanisms are highly dependent on the spacing, density, and distribution of osteons. O'Brien et al. (2005) demonstrated that cracks greater than 300 μm were able to penetrate through osteons. Therefore, while cracks often initiate in the interstitial bone, smaller spacing between adjacent osteons will prevent cracks from reaching a critical length as they will frequently encounter a cement line. However, Taylor also demonstrated that clustering of pores may be detrimental, as cracking may link several pores together, resulting in a larger, more complex pore with a higher stress concentration factor (Hoey & Taylor, 2009).

In trabecular bone, the microarchitecture has been shown to be a significant determinant of mechanical behaviour. Several studies have found bone volume fraction and fabric to be strong determinants of the stiffness and strength of trabecular bone (Maquer et al., 2015; Musy et al., 2017). Additionally, Hernandez et al. (2006) demonstrated that resorption cavities can have detrimental effects on trabecular bone strength beyond what would be expected from the associated decrease in bone volume fraction. It has also been suggested that lacunae within trabecular bone act as stress concentrations sites (McNamara et al., 2006).

Therefore, it is clear that in both cortical and trabecular bone, the microstructure can significantly influence the stress-strain state and directly impact the mechanical properties of the bone. In fact, existing work has demonstrated that a large majority of the observed scatter in the fatigue life of cortical and trabecular bone can indeed be attributed to differences in microarchitecture. In human and bovine cortical bone, previous studies found porosity to negatively correlate with the fatigue life (Carter et al., 1981b; Loundagin et al., 2020; Loundagin & Edwards, 2020; Zioupos et al., 2008). The porosity within cortical bone is largely attributed to the void space created by the vascular network. Previous work demonstrated that the size and spacing of the vascular canals explained a large amount of the fatigue life variation (Loundagin et al., 2020; Loundagin & Edwards, 2020). Additionally, stressed volume was found to be a strong predictor of fatigue life, suggesting that fatigue failure may be predicted by quantifying the stress concentrations associated with the vascular network (Loundagin et al., 2021; Loundagin & Edwards, 2020).

In trabecular bone, existing work found bone volume fraction, fabric, and trabecular thickness to all correlate with the fatigue life (Fatihhi et al., 2015; Rapillard et al., 2006; Topoliński & Mazurkiewicz, 2012). Torres et al. (2019) demonstrated that fatigue failure is highly sensitive

to the proportion of material oriented transverse to the applied load, as these transversely oriented rods act as sacrificial elements to extend fatigue life.

In equine subchondral bone, Martig et al. (2020) found that compressive fatigue life was positively associated with bone apparent stiffness. Additionally, equine subchondral bone exhibits structural differences as a function of distance from the articular surface (Martig et al., 2018). A regional analysis, dividing the subchondral bone samples into three contiguous volumes of interest, found fatigue life to be positively associated with bone volume fraction in the middle and deep regions, but not the superficial region, of the subchondral bone (Martig et al., 2020).

2.5 Summary

Fractures of the equine MCP joint are a significant source of morbidity. These injuries are a direct result of repetitive, high intensity loading of the skeleton during racing and training and there is consensus that they represent a mechanical fatigue phenomenon (Riggs, 1999; Riggs et al., 1999a). While the mechanical fatigue behaviour of subchondral bone from the MC3 has been previously described, there exists a considerable amount of scatter (Martig et al., 2013). Previous work has shown that a large majority of the variation in fatigue life can be attributed to differences in bone microarchitecture (Carter et al., 1981a; Fatihhi et al., 2015; Loundagin et al., 2021; Loundagin & Edwards, 2020; Martig et al., 2020; Rapillard et al., 2006; Topoliński & Mazurkiewicz, 2012; Zioupos et al., 2008). However, a more mechanistic understanding of the relationship between subchondral bone quality and fatigue resistance in the equine MCP joint is lacking, which significantly limits the ability to predict fatigue failure.

The research presented in this thesis utilizes a combination of high resolution μCT imaging, biomechanical testing, and finite element modelling to quantify the influence of

microstructure on the mechanical fatigue behaviour of equine subchondral bone from the MCP joint. The findings from this work will aid in developing a more mechanistic understanding of the fatigue failure process.

Chapter Three

Influence of Microstructure on the Mechanical Fatigue Behaviour of Subchondral Bone

3.1 Introduction

Musculoskeletal injuries are a significant source of lost training time and morbidity in racehorses. Bone injuries account for the majority of fatalities among equine athletes, particularly at the metacarpophalangeal (MCP) joint, where fractures of the third metacarpal (MC3) and proximal phalanx (P1) account for the largest proportion of these fatal bone injuries (Johnson et al., 1994; Rosanowski et al., 2017). Fractures of the MCP joint initiate in the subchondral bone, which refers to the bone tissue underlying the calcified cartilage and includes both the subchondral cortical plate and subchondral trabecular bone. These injuries are believed to be a direct result of the repetitive, high intensity loading of the skeleton during high speed racing and training and there is consensus that fractures at this location represent a mechanical fatigue phenomenon (Colgate & Marr, 2020; Martig et al., 2014; Riggs, 1999, 2002; Riggs et al., 1999a).

Mechanical fatigue is characterized by the accumulation of microdamage as a result of repetitive, cyclic loading (Suresh, 1998). Microdamage may lead to progressive degradation in material properties and, in the absence of adequate repair and remodeling, the eventual failure at loading magnitudes well below the monotonic ultimate strength of the material (Burr et al., 1990; Carter & Hayes, 1977). Martig et al. (2013, 2020) explored the relationship between bone microstructure and the *ex vivo* fatigue behaviour of equine subchondral bone from the MCP joint. In compression, the fatigue life (i.e., number of cycles to failure) exhibited a considerable amount of scatter (Martig et al., 2013) and was positively associated with bone apparent stiffness (Martig

et al., 2020). Additionally, equine subchondral bone exhibited structural differences as a function of distance from the articular surface (Martig et al., 2018). A regional analysis, dividing the subchondral bone samples into three contiguous volumes of interest, found fatigue life to be positively associated with bone volume fraction in the middle and deep regions, but not the superficial region, of the subchondral bone (Martig et al., 2020).

Existing work has demonstrated that a large majority of the observed scatter in the fatigue life of cortical and trabecular bone can be attributed to differences in microarchitecture. Previous studies found porosity to negatively correlate with the fatigue life of cortical bone (Carter et al., 1981b, 1981a; Loundagin et al., 2020; Loundagin & Edwards, 2020; Zioupos et al., 2008), while bone volume fraction and trabecular microarchitecture correlate with the fatigue life of trabecular bone (Fatihhi et al., 2015; Rapillard et al., 2006; Topoliński & Mazurkiewicz, 2012). The porosity of cortical bone is largely attributed to the void space from the vascular network and while these discontinuities within the material serve as barriers to crack growth that may help bone withstand repetitive loading (Launey et al., 2010; Nalla et al., 2003), they also give rise to stress concentration sites that increase the likelihood for crack initiation and propagation. Loundagin et al. (2021) used stressed volume (i.e., the volume of bone stressed above yield) to quantify the stress field surrounding stress concentration features and found this metric to be a better predictor of fatigue life than normalized stress, which fails to capture the stress concentration sites associated with the vascular network.

While the fatigue behaviour of equine subchondral bone from the MC3 has previously been described in very good detail (Martig et al., 2013, 2020), a more mechanistic understanding of the relationship between subchondral bone quality and fatigue resistance is lacking, which significantly limits the ability to predict fatigue failure at the MCP joint. There is also a dearth of

information regarding the mechanical fatigue behavior of bone from the P1, despite the fact that this bone is also prone to fracture (Johnson et al., 1994; Rosanowski et al., 2017, 2019). Therefore, the objective of this work was to quantify the influence of bone microarchitecture on the mechanical fatigue behaviour of equine subchondral bone from both the MC3 and P1. Our primary aim was to determine if stressed volume can predict fatigue life better than normalized stress (i.e., initial nominal strain). Our secondary aim was to establish the relationship between stressed volume and microarchitecture at different regions throughout subchondral bone from the MCP joint. We hypothesized that stressed volume would predict fatigue life better than normalized stress and that a higher stressed volume would be associated with lower bone volume fraction.

3.2 Methods

3.2.1 Specimen Collection and Preparation

Twelve equine forelimbs were harvested from 8 horses euthanized for reasons unrelated to this research. This research was approved by our institutional ethics board through a "Statement of Animal Tissue or Cadaver Use" protocol (Ethics ID: #AC20-0152). Similar to Martig et al. (2013), the palmar aspect of the MC3 was removed with a bandsaw by cutting at an angle of 55° in the frontal plane in a palmaro-proximal to dorso-distal direction. The distal end of the P1 was also removed with a bandsaw by cutting parallel to the articular surface. Cylindrical bone samples measuring 6.7 mm in diameter were extracted from the medial and lateral condyles of the MC3 and P1 using a drill press, yielding 4 samples per limb, for a total of 48 subchondral bone samples (Figure 3-1). A precision saw was then used to remove the cartilage, resulting in a minimal yet unquantified loss of subchondral bone. The samples were cut to a length of approximately 8 mm and polished using 600 grit sandpaper to ensure surfaces were planoparallel. Specimens were then wrapped in gauze soaked in phosphate buffered saline (PBS) and stored in a -30°C freezer.

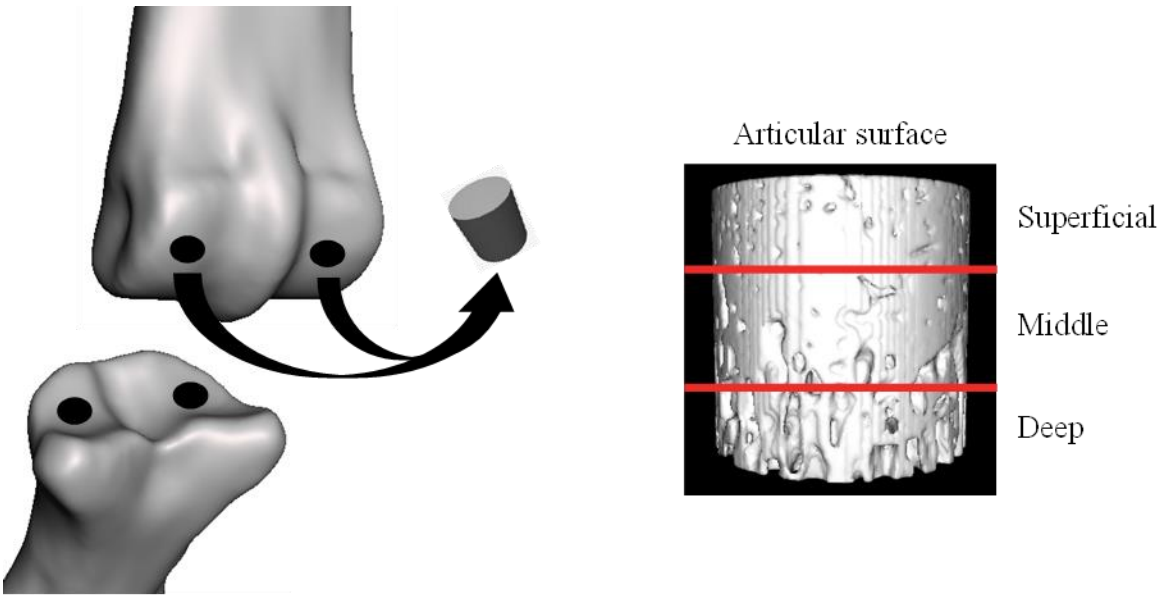

Figure 3-1: (Left) Samples were collected from the medial and lateral condyles of the MC3 towards the palmar aspect and from the medial and lateral condyles of the P1. (Right) Samples were divided into three contiguous regions of equal length for further analysis.

3.2.2 Micro-Computed Tomography

Samples were thawed and imaged using a Scanco μCT 35 scanner (Scanco Medical AG, Bassersdorf, Switzerland) with an isotropic voxel size of 6 μm. Scans were acquired with an x-ray tube voltage and current of 55 KVp and 145 μA, respectively, and an integration time of 500 ms. After scanning, samples were rehydrated and wrapped in gauze soaked in PBS before being stored in a -30°C freezer. Images were cropped such that a region of interest 6 mm in diameter and 6 mm in length (measured from the articular surface) was used for image analysis to avoid machining artifacts at the surface of the sample and to maintain consistency. Image stacks were segmented via intensity-based thresholding using MATLAB (r2021b, Mathworks, MA, USA) (Figure 3-2). The threshold value for bone was identified as 70% of the mode of pixel intensities throughout the image. Microarchitecture was quantified using the Fiji software package (v2.9.0, NIH, USA)

(Schindelin et al., 2012). Bone volume fraction was calculated as the fraction of bone volume to total volume. Tissue mineral density and apparent bone mineral density were calculated using a calibration phantom to establish the relationship between CT pixel intensity and mineral density. Pore size and pore spacing were determined using the thickness and separation options included in the BoneJ plugin (Doube et al., 2010). To determine the number of pores in the entire sample, images were skeletonized, and the number of pores was calculated as the number of junctions in the skeleton plus one. For direct comparison with previous research (Martig et al., 2020), we also performed a regional analysis to quantify microarchitectural parameters in three successive regions, each 2 mm in length (superficial, middle, and deep) (Figure 3-1).

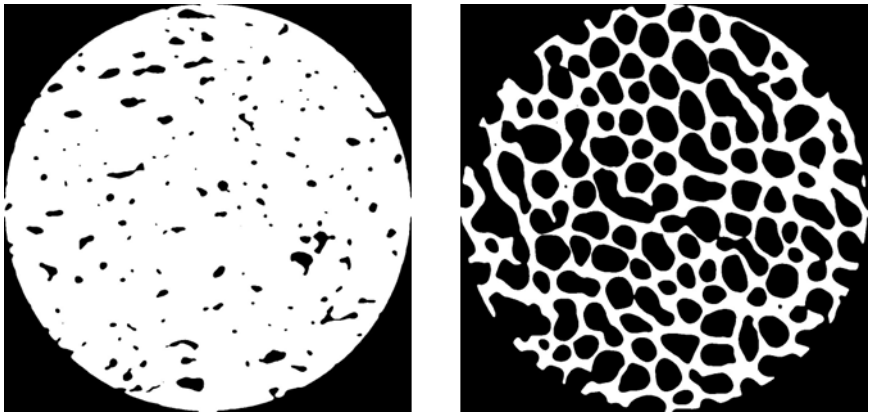

Figure 3-2: Segmented images from the (left) superficial, subchondral cortical plate and (right) deep, subchondral trabecular bone.

3.2.3 Biomechanical Testing

Samples were thawed and rehydrated in PBS at room temperature for two hours prior to testing. The proximal (i.e., trabecular) end of each sample was potted with bone cement into a lower platen with a 2 mm deep central hole (Martig et al., 2013) (Figure 3-3). The articular surface was left unconstrained in contact with a flat upper platen fixed to a 10 kN load cell in line with the

actuator of the materials testing machine (ElectroPuls E10000, Instron, Norwood, MA, USA). After potting, the exposed length of the specimen was recorded for strain and modulus calculations. Samples were tuned based on stiffness to a stress of 23 MPa (20% of yield strength) and fatigue life was assessed by cyclically loading samples between 0.8 and 70 MPa of compression (apparent stress based on the nominal diameter) under load control at a frequency of 2 Hz. Samples were loaded at this frequency to mimic physiological stride frequency at racing speed and to facilitate comparison with the literature (Martig et al., 2013; Morrice-West et al., 2021; Takahashi et al., 2021). Pilot work also demonstrated no difference in fatigue life for samples from the MCP joint when loaded at 2 Hz and 0.2 Hz (Appendix A). Data was collected every cycle for the first 100 cycles, then for 10 cycles every 100 cycles up to 1000 cycles, and for 10 cycles every 1000 cycles until the completion of the test. Normalized stress was determined by dividing the applied stress by the initial modulus. The initial elastic modulus was taken from the 10^{th} loading cycle and fatigue life was identified as the cycle with the lowest recorded stiffness. Energy loss per unit volume was computed by taking the difference in area between the loading and unloading portion of the stress-strain curve. Similar to Haider et al. (2023), since data was collected intermittently at progressively longer intervals over the test duration, total energy dissipation was calculated by summing energy dissipation for all cycles, using linear interpolation to estimate dissipation for cycles where the hysteresis loops were not recorded.

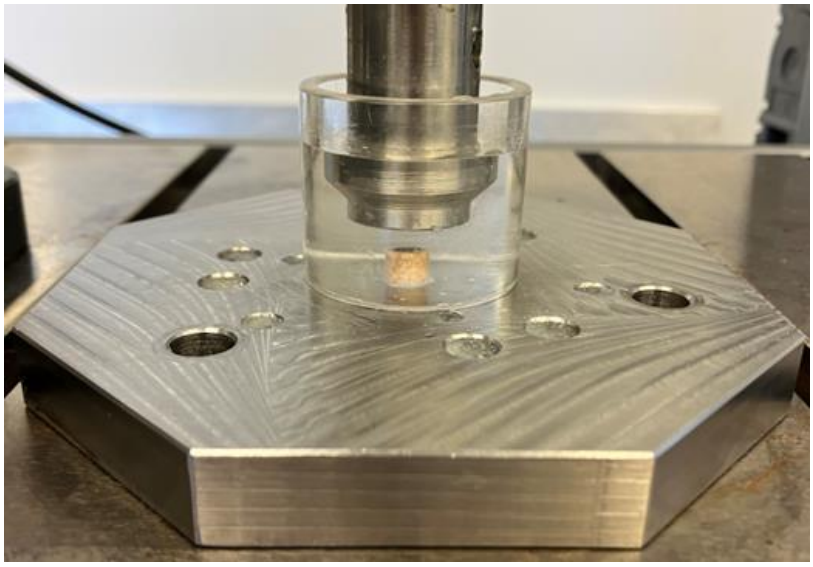

Figure 3-3: Experimental fatigue testing setup

3.2.4 Finite Element Modelling

Finite element models were developed from the cropped and segmented μCT images to quantify the volume of bone stressed above yield for each sample using FAIM software (v8.0, Numerics88 Solutions Ltd., Canada). μCT elements from the thresholded image were coarsened to a voxel size of 24 μm and converted to linear hexahedral elements. A mesh convergence analysis confirmed that the model was sufficiently converged at this element size, as a 0.5% change in the stressed volume was observed when the element size was halved. Elements were assigned homogeneous, linear-elastic material properties with a Poisson's ration of 0.3. Tissue modulus was applied such that the apparent modulus of the finite element model matched the apparent modulus of the corresponding experimentally tested sample. The tissue modulus values applied to the model had a mean ± SD of 4.8 ± 0.7 GPa. The boundary conditions were consistent with experimental testing protocols, with a uniform compressive load of 1979 N distributed over the entire

subchondral surface and the proximal surface nodes fixed. The stressed volume was defined as the volume of material experiencing a von Mises stress greater than the yield strength of equine subchondral bone, which was assumed to be 115 MPa (Rubio-Martínez et al., 2008) (Figure 3-4).

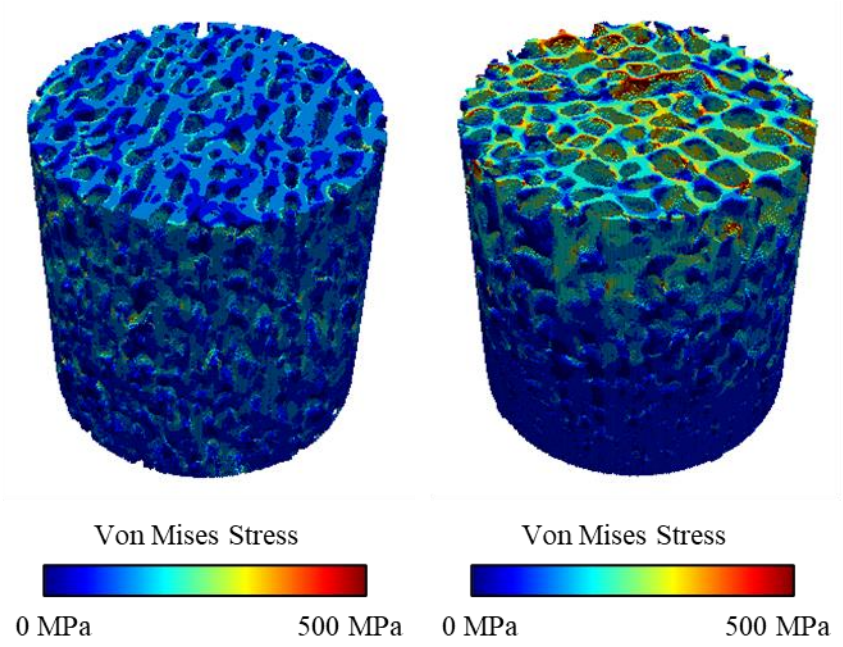

Figure 3-4: Finite element predicted stress distribution of an equine subchondral bone sample from the (left) MC3 and (right) P1 loaded in compression. The articular surface is oriented towards the bottom of the figure.

3.2.5 Statistical Analysis

To examine the relationship between fatigue life and microarchitectural variables while accounting for potential horse specific effects, a Bayesian, frailty model with Weibull baseline hazard was utilized (Hougaard, 2000; Ibrahim et al., 2001). For each microarchitectural parameter, a model containing fixed effects for the architectural parameter of interest, bone location (MC3 and P1) and their interaction along with a multiplicative random effect for horse was fit to observed failure times using probabilistic programming language Stan (Carpenter et al., 2017). Evidence for

an effect of microarchitecture, bone location or their interaction was assessed via examination of the marginal posterior for these effects. In addition, comparison of root mean squared error (RMSE) as well as expected log point-wise predictive density (ELPD) - a measure of prediction accuracy if the model were to be applied outside of the current data set (Vehtari et al., 2017) - were made. If zero fell outside of two standard errors of the expected difference in ELPD between the full model and that of a null model (without architectural parameter included) it was concluded that the microarchitectural parameter was likely to have a significant effect on fatigue life. To interpret the effect, plots of the survival probability given loading cycles for varying levels of the parameter were produced using R (v. 4.2.1, R Core team). Full details of this statistical modelling procedure can be found in Appendix B.

A secondary, exploratory analysis investigating the relationship between fatigue life, stressed volume, normalized stress, and microarchitectural parameters at different regions throughout the subchondral bone was conducted using frequentist statistics to facilitate comparison with existing literature (Martig et al., 2020). The Shapiro-Wilk test of normality was used to determine the distribution of the experimental variables. While the majority were normally distributed, MC3 stressed volume, whole MC3 pore spacing, superficial MC3 pore size, middle MC3 pore spacing, and middle P1 pore spacing were not. Pearson product-moment correlations were used to examine the relationships between experimental variables. Spearman rank-order correlations were also used to examine relationships for non-normally distributed data, but they did not provide a different interpretation of the relationships. Therefore, Pearson's correlations are reported throughout with $\alpha = 0.05$. Statistical analysis was performed in R (v. 4.2.1, R Core team).

3.3 Results

Two quarter horses, three standardbred horses, and three thoroughbred horses were used in this study. Three of the eight horses were male geldings, and the remaining five horses were female. The horses ranged in age from two years old to 25 years old and had a variety of training backgrounds. Demographic information is summarized in Table 3-1.

Table 3-1: Demographic information of horses. Only an estimate of the age of the first horse was available and the athletic history was not known.

Horse	Age (years)	Sex	Breed	Left or Right Forelimb	Athletic History
1	18-25	Male (gelding)	Quarter horse	Both	
2	18	Female	Quarter horse	Right	Previously competitive cow horse
3	2	Male (gelding)	Standardbred	Both	Racehorse
4	20	Female	Thoroughbred	Left	Previously athletic polo horse
5	25	Female	Thoroughbred	Left	Previously athletic polo horse
6	13	Male (gelding)	Thoroughbred	Left	Racehorse
7	2	Female	Standardbred	Both	Racehorse
8	3	Female	Standardbred	Both	Racehorse

Results from the μCT analysis, mechanical testing, and finite element modelling are summarized in Table 3-2 and Table 3-3. Three samples were removed from the analysis as they failed during the first loading cycle. These samples were collected from the lateral condyle of the P1 from horse 7 (right forelimb) and horse 8 (left and right forelimbs).

Table 3-2: Median and range (min-max) of μCT derived microstructural parameters and material properties

	Tissue Mineral Density (mg/cm^3)	Bone Mineral Density (mg/cm^3)	BVF (%)	Mean Pore Size (μm)	Mean Pore Spacing (μm)	Number of Pores
MC3	916.3 *(880.2-1007.5)*	757.5 *(661.0-894.3)*	76.5 *(60.7-89.5)*	192.0 *(126.4-263.1)*	265.7 *(222.6-395.6)*	8702 *(6048-14051)*
P1	927.8 *(866.0-990.5)*	729.6 *(634.8-836.1)*	72.1 *(63.8-81.8)*	289.6 *(194.6-356.7)*	322.2 *(243.2-406.5)*	6338 *(4237-11688)*
Pooled	919.9 *(866.0-1007.5)*	747.1 *(634.8-894.3)*	73.0 *(60.7-89.5)*	242.8 *(126.4-356.7)*	288.0 *(222.6-406.5)*	7629 *(4237-14051)*

Table 3-3: Median and range (min-max) of mechanical measurements

	Fatigue Life (Cycles)	Stressed Volume	Normalized Stress
MC3	1479 *(21-40082)*	0.20 *(0.02-0.59)*	0.023 *(0.018-0.032)*
P1	1875 *(71-35766)*	0.27 *(0.13-0.45)*	0.028 *(0.020-0.039)*
Pooled	1775 *(21-40082)*	0.25 *(0.02-0.59)*	0.025 *(0.018-0.039)*

The statistical model represented the data well for the chosen parameters, as can be seen in Figure 3-5. Based on RMSE, bone volume fraction was the best predictor of fatigue life, followed by stressed volume and apparent bone mineral density. When using ELPD to evaluate the models, stressed volume illustrated the best predictive performance, followed by bone volume fraction and apparent bone mineral density (Figure 3-5). When taken together, the results from the RMSE and ELPD make it difficult to conclude whether stressed volume or bone volume fraction was a better predictor of fatigue strength, but both were definitively better predictors than normalized stress and tissue mineral density. When MC3 and P1 samples were analyzed separately, statistical analysis revealed that while stressed volume was a better predictor of fatigue life than normalized stress for P1 samples, stressed volume and normalized stress were equally predictive of fatigue failure in MC3 samples.

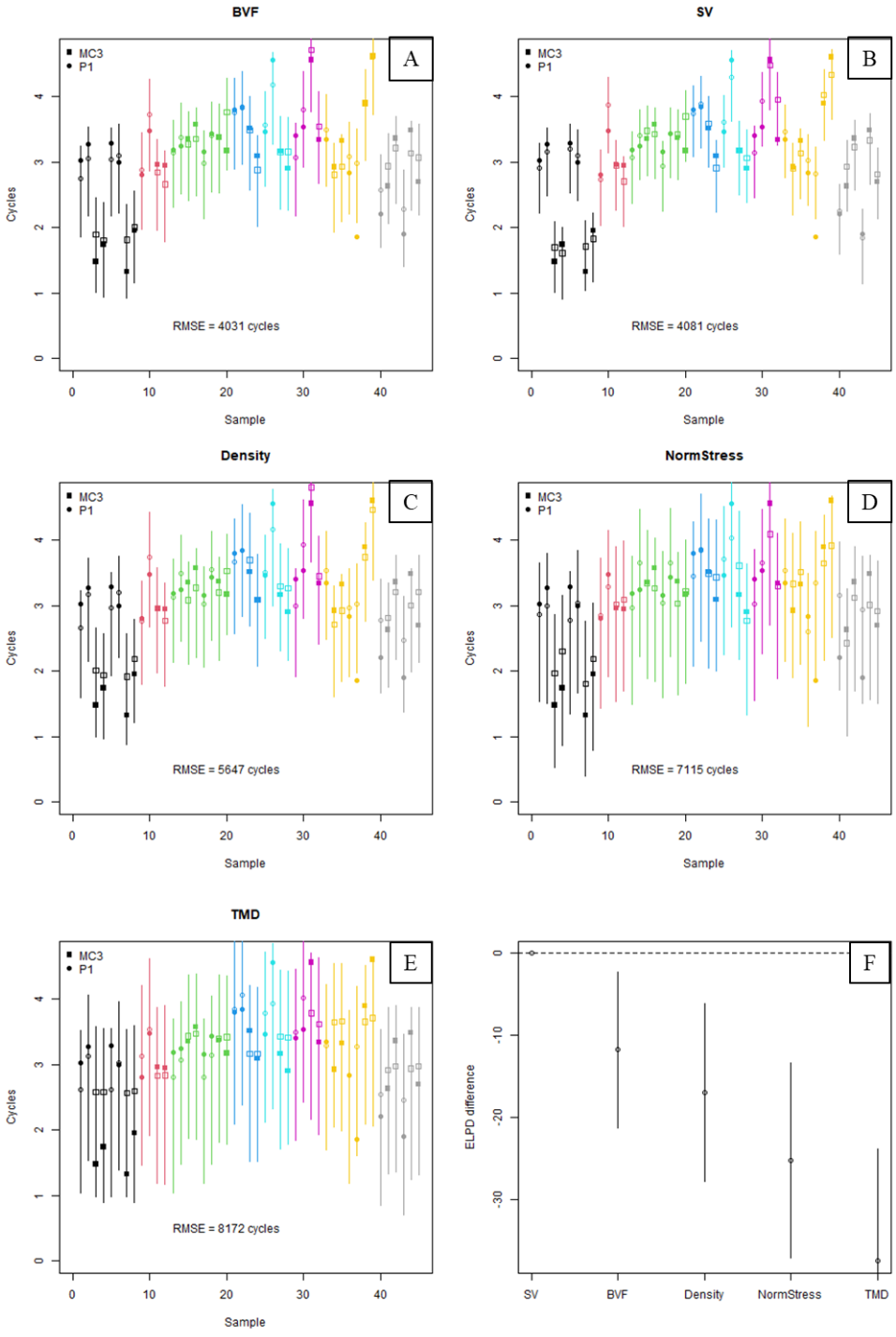

Figure 3-5: A plot of predicted (hollow) cycles to failure (log10 scale) vs observed (solid) along with the 95% confidence interval (vertical line), coloured by horse for (A) BVF = bone volume fraction, (B) SV = stressed volume, (C) Density = apparent bone mineral density, (D) NormStress = normalized stress, and (E) TMD = tissue mineral density. (F) is a measure of expected leave out predictive performance with bars representing 2 standard errors between each model and the best model (i.e., stressed volume).

Survival curves from the statistical model representing the survival probability of a MC3 or P1 sample are shown in Figure 3-6. Existing work found horses that experienced a fracture travelled an average of 37.4 km in the 30 days prior to the injury (32.9 km at a canter and 4.5 km at a gallop) (Verheyen et al., 2006). Assuming a canter stride length of 5.7 m and a gallop stride length of 7.3 m (Takahashi et al., 2021), this would correspond to approximately 6500 loading cycles. The median stressed volume for MC3 samples was 23% lower than for P1 samples. This decrease in the stressed volume corresponded to an increase in the likelihood of surviving 6500 cycles by 200%. While a sample from the MC3 is expected to survive longer than a sample from the P1 based on the median stressed volume, expected survival times are nearly identical when considering normalized stress.

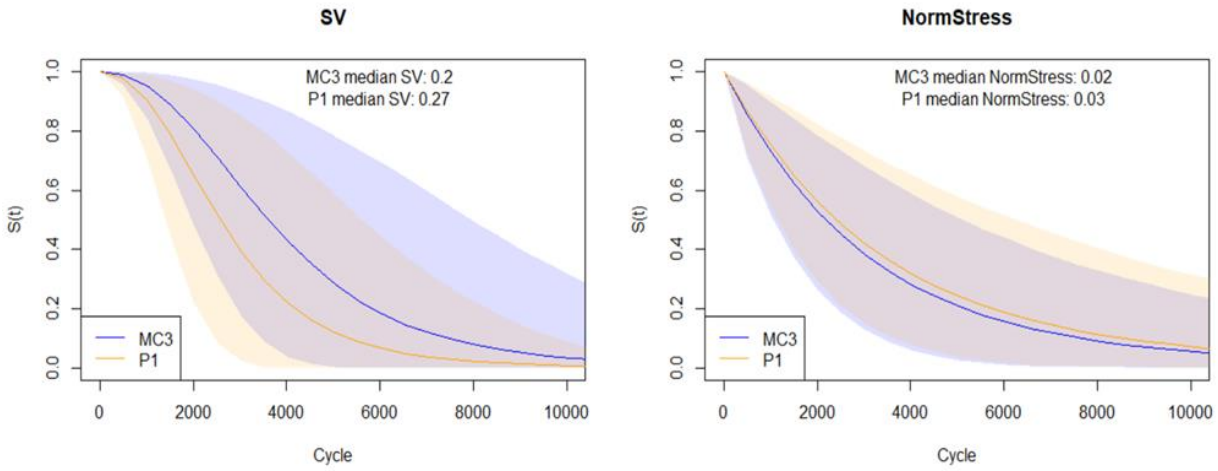

Figure 3-6: Survival curves representing the likelihood of survival probability vs cycles to failure for an average horse for a MC3 or P1 bone at the median value of the variable of interest for that particular bone.

While bone volume fraction was a strong predictor of fatigue life in both bones, each bone displayed drastically different microarchitecture. MC3 samples illustrated a relatively consistent bone volume fraction throughout the length of the sample, while P1 samples were much more heterogeneous (Figure 3-7). Additionally, when defining trabecular bone as having a bone volume fraction less than 50%, P1 samples contained trabecular bone in the deep region, while MC3 samples were composed predominantly of the cortical plate throughout.

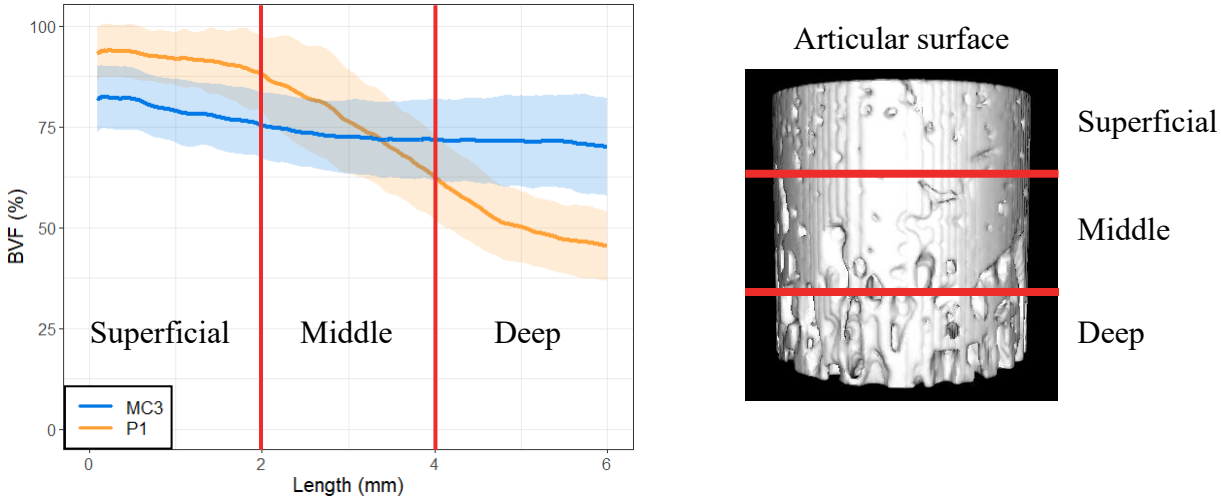

Figure 3-7: A plot of bone volume fraction as a function of the length of a sample. Curves represent the mean of all samples for the particular bone, with shaded regions representing one standard deviation.

Correlations between fatigue life, stressed volume, normalized stress, and regional bone volume fraction measurements are summarized in Table 3-4. Regionally, the fatigue life was positively associated with BVF in all regions for the MC3 and with BVF in the superficial and middle regions for the P1. Stressed volume was more strongly correlated with BVF in the middle and deep regions for the MC3 and with BVF in the middle region for the P1. Normalized stress

was correlated with BVF in all regions for the MC3 and with BVF in the middle and deep regions for the P1.

Table 3-4: Relationship between fatigue life (N_f), stressed volume, normalized stress, and regional bone volume fraction measurements. R^2 values are reported. Bold values have $p < 0.05$.

		Total BVF	Superficial BVF	Middle BVF	Deep BVF
$\log(N_f)$	MC3	**0.80**	**0.72**	**0.72**	**0.55**
	P1	**0.49**	**0.25**	**0.71**	0.10
Stressed Volume	MC3	**0.95**	**0.57**	**0.90**	**0.84**
	P1	**0.84**	**0.37**	**0.95**	**0.34**
Normalized Stress	MC3	**0.41**	**0.41**	**0.37**	**0.27**
	P1	**0.33**	0.01	**0.36**	**0.25**

Correlations between fatigue life, stressed volume, normalized stress, and regional microstructural measurements are summarized in Table 3-5. At the microstructural level, fatigue life, stressed volume, and normalized stress were more strongly associated with the size of the pores rather than the number of bone pores present.

Table 3-5: Relationship between fatigue life (N_f), stressed volume, normalized stress, and regional microstructural measurements. R^2 values are reported. Bold values have $p < 0.05$.

		Whole Sample			Superficial Region		Middle Region		Deep Region	
		Average Pore Size	Average Pore spacing	Number of Pores	Average Pore Size	Average Pore spacing	Average Pore Size	Average Pore spacing	Average Pore Size	Average Pore spacing
$\log(N_f)$	MC3	**0.53**	**0.48**	0.05	**0.42**	**0.28**	**0.54**	**0.43**	**0.40**	**0.47**
	P1	0.14	0.03	0.05	**0.37**	0.01	**0.47**	0.09	0.15	0.01
Stressed Volume	MC3	**0.56**	**0.55**	0.01	**0.33**	**0.18**	**0.52**	**0.54**	**0.58**	**0.71**
	P1	**0.25**	0.10	0.03	**0.77**	0.01	**0.57**	**0.30**	**0.25**	0.11
Normalized Stress	MC3	**0.33**	**0.23**	0.09	**0.33**	0.13	**0.31**	**0.19**	**0.21**	**0.25**
	P1	**0.30**	0.04	**0.25**	**0.37**	0.17	**0.39**	0.01	**0.23**	0.05

3.4 Discussion

The fatigue life of equine subchondral bone exhibits a significant amount of variability dependent, in part, on bone microarchitecture. Previous work has explored the relationship between the fatigue behaviour and microstructure of subchondral bone from the MCP joint (Martig et al., 2013, 2020) but a mechanistic understanding of the relationship between bone quality and fatigue resistance is still lacking. In this study, stressed volume was a strong predictor of fatigue life in both the MC3 and P1, with a higher stressed volume being associated with a lower fatigue life. Stressed volume was a better predictor of fatigue life than normalized stress in the P1, but they were equally predictive in the MC3. Regionally, fatigue life was positively associated with bone volume fraction in all regions of the MC3, but only in the superficial and middle regions of the P1. By identifying the microstructural features most relevant to fatigue resistance in equine subchondral bone, this work begins to develop a fundamental understanding of the underlying mechanisms of the fatigue failure process in the equine MCP joint.

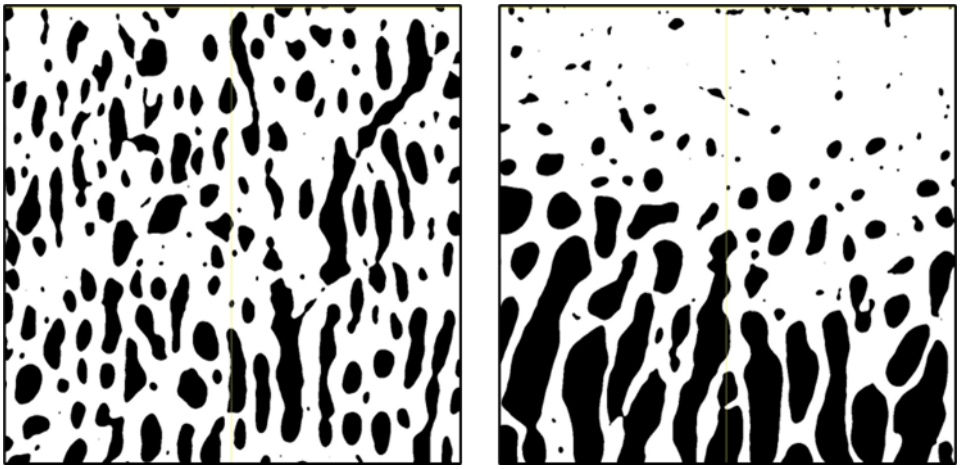

Figure 3-8: Cross sectional image of a (left) MC3 sample and a (right) P1 sample. The articular surface is oriented towards the top if the image.

In this study, we hypothesized that stressed volume would be a better predictor of fatigue life than normalized stress. While this was the case for P1 samples, it did not hold true for samples from the MC3. This discrepancy can likely be attributed to differences in microarchitecture homogeneity (Figure 3-7; Figure 3-8). The microstructure of the MC3 was quite homogeneous in nature and the normalized stress accounting for elastic modulus was an accurate representation of the initial strain state experienced throughout the entire sample and was therefore a good predictor of fatigue life. On the other hand, the P1 microstructure was a function of sample length and the initial modulus was significantly correlated with bone volume fraction in the middle and deep regions. This means the initial modulus of P1 samples was largely driven by the trabecular bone underlying the cortical plate. Indeed, during mechanical testing, P1 samples often exhibited a much larger initial displacement compared to MC3 samples (Figure 3-9). This behaviour can likely be attributed to the progressive collapse of the trabecular network. After the trabecular bone quickly collapses, the displacement profile flattens out as the subchondral cortical plate is left to bear the majority of the load for the remainder of the test. Thus, while the initial modulus has been shown to have a strong, positive correlation with fatigue life (Carter et al., 1981b; Loundagin et al., 2020), the initial modulus, and therefore the normalized stress, of the P1 samples was largely driven by the trabecular bone underlying the cortical plate, whereas failure was associated with fracture of the cortical plate. This notion that final failure is associated with fracture of the cortical plate is further supported by the fact that the regional analysis indicated no significant relationship between the fatigue life of samples from the P1 and bone volume fraction in the deep region, which was predominantly trabecular bone. Taken together, these results suggest that the subchondral cortical plate plays a more prominent role in the fatigue resistance compared to the underlying trabecular bone.

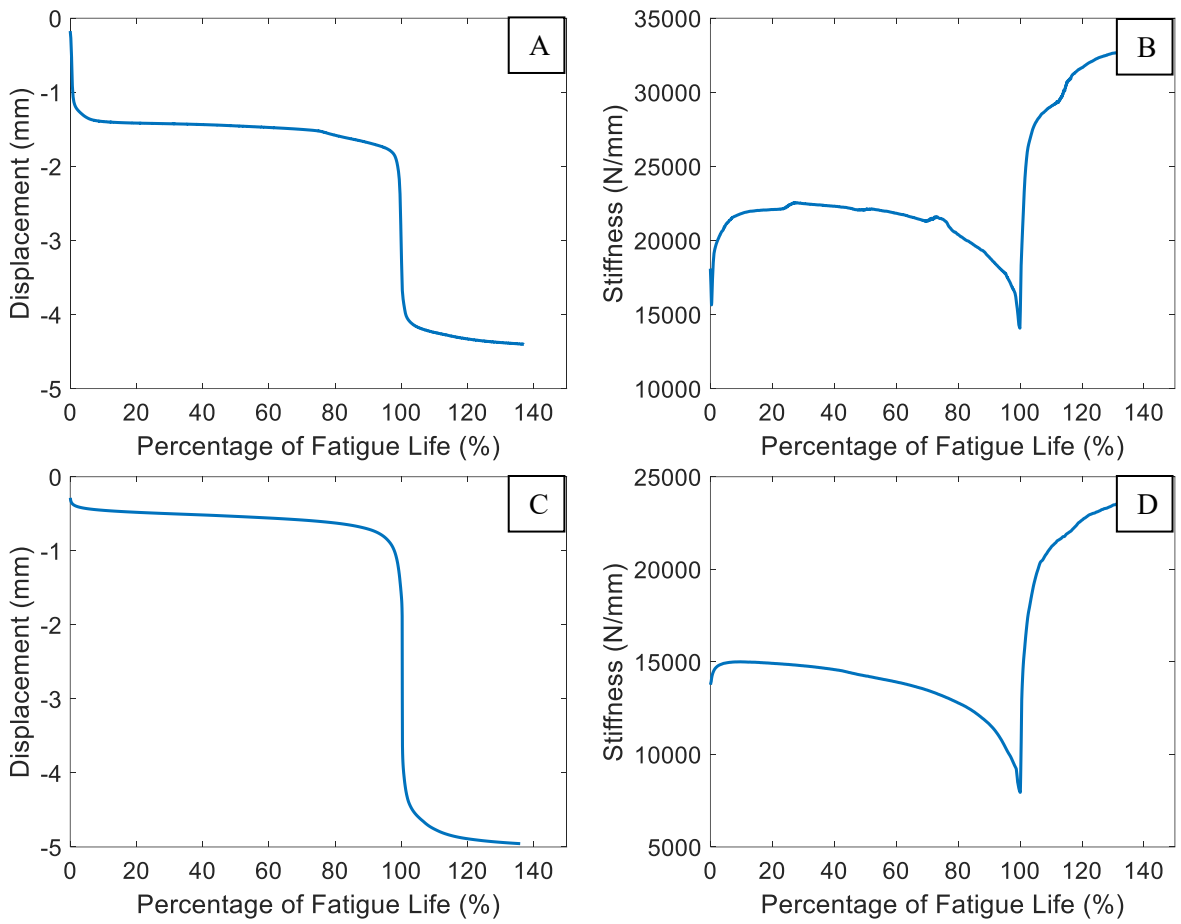

Figure 3-9: Representative displacement and stiffness profiles from a P1 sample (A, B) and MC3 sample (C, D). P1 samples illustrated a larger initial decrease in displacement that can likely be attributed to the collapse of the trabecular network.

Stressed volume was associated with both pore size and spacing in MC3 samples, but it was more strongly correlated with pore size than pore spacing in P1 samples. Given that the MC3 samples were predominantly composed of the cortical plate, the stressed volume was largely dictated by the size and distribution of the vascular canals. While bone is known to accumulate microdamage in response to loading, it is the resistance to the propagation of microcracks that is critical in avoiding fracture (O'Brien et al., 2003). Larger pores will subject a larger volume of

material to an elevated stress, and therefore increase the ability of a microcrack to grow within the bony matrix. While pore separation can influence fatigue behaviour through toughening mechanisms, (Nalla et al., 2005; O'Brien et al., 2005), only the first loading cycle was modelled in the finite element analysis, meaning any toughening mechanisms are not captured. Instead, a smaller pore separation may cause multiple stress concentrations to interact. While the effect of interacting stress concentrations is highly complex and dependent on both geometry and mode of loading (Davis et al., 2017; Graham et al., 2005), these interactions may amplify local stresses and cause elements that would otherwise experience stresses below yield to now experience elevated stresses exceeding the threshold value. In the P1 samples, the superficial region is composed of the cortical plate. Compared to the MC3 samples, this region had smaller pores spaced further apart. Therefore, the lack of relationship between stressed volume and pore spacing in the superficial region of P1 samples may be due to the fact that pores were spaced sufficiently far away from one another to limit any interactions. In the deep region of the P1 samples, the correlation between stressed volume and pore spacing (i.e., trabecular thickness) was not significant, while the relationship with pore size (i.e., trabecular spacing) was significant but weak. Given that previous work has shown measures of bone volume fraction and fabric to have important implications on the mechanical properties of trabecular bone, a metric quantifying the orientation of the trabecular bone within P1 samples may be needed to explain more of the variation (Maquer et al., 2015; Musy et al., 2017).

Our regional analysis suggested that fatigue was most strongly associated with bone volume fraction in the superficial and middle regions of the subchondral bone samples. Martig et al. (2020) found fatigue life to be positively associated with bone volume fraction in the middle and deep regions of the subchondral bone. This discrepancy can likely be attributed to differences

in the microstructure of the samples. While Martig et al. (2020) only examined samples from the MC3 and reported mean bone volume fraction measurements ranging from 97% in the superficial region to 90% in the deep region, the MC3 samples used in this study had a mean bone volume fraction of 79% in the superficial region and 71% in the deep region, while P1 samples had a mean bone volume fraction of 92% in the superficial region and 51% in the deep region with some samples reaching bone volume fraction as low as 34% in the deep region. The marked difference in bone volume fraction, particularly in the deep region, demonstrates how structurally different our samples were from the samples of Martig et al. (2020). These structural differences can likely be attributed to differences in the equine populations from which the samples were drawn. While Martig et al. collected samples exclusively from thoroughbred racehorses, the horses used in this study included quarter horses and standardbreds in addition to thoroughbreds, not all of which were racehorses. Samples from Martig et al. (2020) also included a larger proportion of immature horses (less than 4 years old) which is important to consider given immature horses illustrate differences in bone composition compared to mature horses, such as lower bone mineral density (Van Der Harst et al., 2005). Therefore, these demographic differences must be considered when comparing results from these studies.

In the primary statistical analysis, a frailty model was implemented to account for the fact that samples from the same horse are likely to behave more cohesively than samples from different horses. A frailty term less than one indicates that samples from that horse would fail sooner than expected. As can be seen in Figure 3-10, the lowest frailty terms were associated with horses 1, 3, 7, and 8. Interestingly, horses 3, 7, and 8 were the three youngest horses and were all standardbreds. It should be noted that thoroughbreds and standardbreds compete in considerably different race types that best suit their specific traits and strengths. While thoroughbreds compete in flat racing

and travel at an intense gallop, standardbreds compete in harness racing, where they race at a trotting speed. These different race types will inevitably influence the loading environment within the MCP joint and may also lead to different skeletal adaptations. Indeed, geometric differences of the MC3 bones from thoroughbred and standardbred racehorses have been identified (Nunamaker et al., 1989). Therefore, the results suggest that these differences may influence their fatigue resistance and resulting fracture risk.

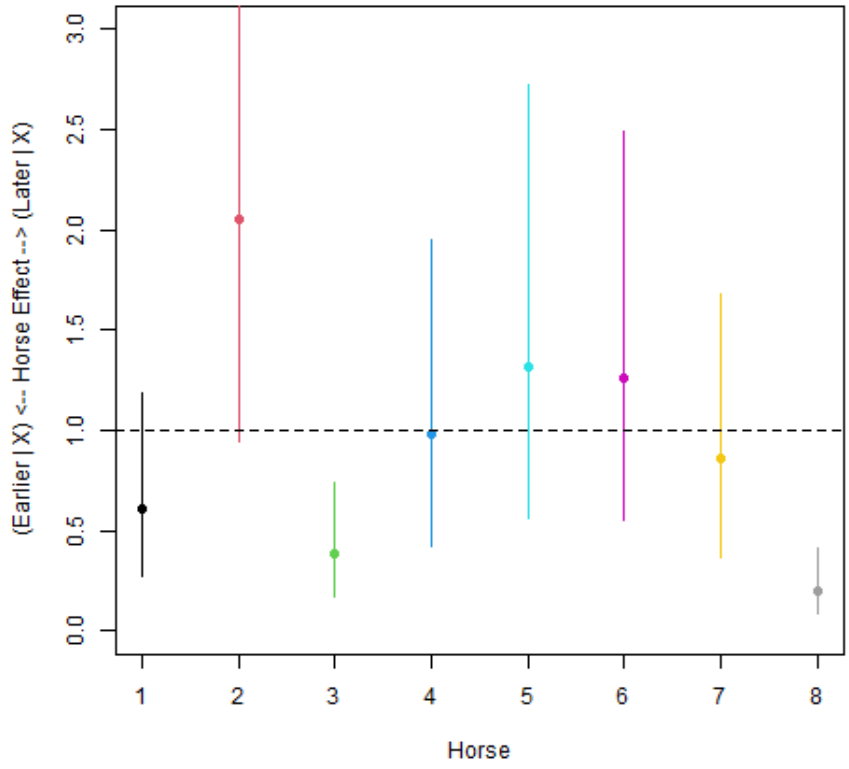

Figure 3-10: Frailty terms for each horse. A value of less than one indicates that samples from that horse failed earlier than expected.

This work demonstrates that subchondral bone microstructure may be used to predict fatigue life. The microarchitectural features identified in this work were detected with a scan

resolution of 6 μm. Clinically, while standing equine CT of the distal limb can achieve sub-millimeter resolution, this is insufficient to be able to detect microstructural features described throughout this study. However, the bone biomarkers identified in this research as being the most important determinants of fatigue strength may be used to inform appropriate screening measures for equine bone health as more advanced imaging methods become clinically available. Alternatively, apparent bone mineral density may be a more accessible option given that this metric was also a strong predictor of fatigue life and can be readily obtained from a clinical CT scan. Additionally, the finite element modelling applied in this work was limited to linear elastic assumptions and only modelled the first loading cycle, thus neglecting the influence of damage accumulation on material property degradation. While the deep region of the P1 samples contained trabecular bone, the transition from cortical bone to trabecular bone was not always clear as it was difficult to distinguish between porous cortical bone and dense trabecular bone. Additionally, while the results suggest that the cortical plate may play a more important role in the fatigue resistance of subchondral bone from the MCP joint, the importance of the trabecular bone cannot be discounted. Indeed, previous work investigating the failure behaviour of rat vertebrae found that the combined contributions of both the cortical shell and trabecular bone must be considered as compressive failure was associated with stress concentrations sites in the cortical shell coupled with a reduced trabecular bone volume adjacent to the stress concentration sites (Morton et al., 2018).

In summary, this work used a combination of high-resolution microCT imaging, biomechanical testing, and finite element modelling to quantify the influence of microarchitecture on the fatigue behaviour of equine subchondral bone. While stressed volume was a strong predictor of fatigue life in both the MC3 and P1, normalized stress was equally predictive of fatigue life for

MC3 samples. This can be attributed to the more homogeneous nature of the MC3 microstructure. Fatigue life was more strongly correlated with bone volume fraction in the superficial and middle regions of the subchondral bone, suggesting that the cortical plate plays a more prominent role in the fatigue resistance. By improving our understanding of the variance in fatigue life measurements, this research helps begin to clarify the underlying mechanisms of the mechanical fatigue process and provide a basic understanding of subchondral bone injuries in the equine fetlock joint.

Chapter Four

Conclusions

4.1 Summary

Musculoskeletal injuries are a significant source of lost training days and morbidity in racehorses. The MCP joint experiences some of the highest loads of the distal limb and is the most frequently injured site (Harrison et al., 2010; Rosanowski et al., 2017). Fractures at this location initiate in the subchondral bone and are believed to be a direct result of the repetitive, high intensity loading of the skeleton during racing and training. Therefore, there is consensus that these injuries represent a mechanical fatigue phenomenon. While the fatigue behaviour of subchondral bone from the MCP joint has been previously described (Martig et al., 2013, 2020), there exists a significant amount of scatter within the data that can be attributed to the inherent variability in bone microarchitecture.

The objective of this work was to quantify the influence of microstructure on the mechanical fatigue behaviour of subchondral bone from the equine MCP joint using a combination of high-resolution μCT imaging, biomechanical testing, and finite element modelling. Our primary aim was to determine if stressed volume could predict fatigue life better than normalized stress. Our secondary aim was to establish the relationship between stressed volume and microarchitecture at different regions throughout subchondral bone from the MCP joint. We hypothesized that stressed volume would predict fatigue life better than normalized stress and that a higher stressed volume would be associated with lower bone volume fraction.

Stressed volume was a strong predictor of fatigue life in both the MC3 and P1, with a higher stress volume being associated with a lower fatigue life. Normalized stress was also a strong

predictor of fatigue life for MC3 samples, but not for P1 samples. This disparity can be attributed to the more homogeneous nature of the MC3 microstructure. Fatigue life was more strongly correlated with bone volume fraction in the superficial and middle regions of the subchondral bone, suggesting that the cortical plate plays a more prominent role in the fatigue resistance of subchondral bone from the MCP joint. By improving our understanding of the variance in fatigue life measurements, this research begins to clarify the underlying mechanisms of the mechanical fatigue process and provides a basic understanding of subchondral bone injuries in the equine MCP joint.

4.2 Strengths

This work has several novel and unique aspects that were able to address existing gaps in this area of research. Previous work describing the compressive fatigue behaviour of equine subchondral bone only used samples from mature horses (greater than 4 years of age) (Martig et al., 2013) even though MCP fractures are often seen in 2 – 4 year old racehorses (Johnson et al., 1994). Additionally, there exist age-related differences in bone composition that may influence fatigue life. For instance, existing work has demonstrated that immature horses illustrate lower bone mineral density and calcium content (Van Der Harst et al., 2005). Previous work also only used samples from thoroughbred racehorses, despite the fact that other breeds also experience these injuries (Johnson et al., 1994). Therefore, this work is novel in that it used both mature and immature horses, and also collected samples from a variety of breeds.

Although both the MC3 and P1 are prone to fracture (Johnson et al., 1994; Rosanowski et al., 2017, 2019), existing work has focused on describing the fatigue behaviour of equine subchondral bone from the MC3 only (Martig et al., 2013, 2020; Shaktivesh et al., 2020). Therefore, this work was able to improve upon the existing research by quantifying the fatigue

behaviour of subchondral bone from both the MC3 and P1. Additionally, this work illustrated disparate results between the MC3 and P1, highlighting the importance of investigating the fatigue behaviour of both bones.

While previous work has investigated the influence of microstructure on the mechanical fatigue behaviour of equine subchondral bone, it was limited to few microstructural measures. Specifically, previous work only quantified bone volume fraction and tissue mineral density (Martig et al., 2020). Although this helped develop an understanding of the importance of bone volume fraction, a mechanistic understanding of the relationship between bone quality and fatigue resistance in equine subchondral bone was still lacking, which significantly limited our ability to predict fatigue failure. Our work was able to go beyond simple measures of bone volume fraction by quantifying the size and distribution of pores within the samples, which have been shown to correlate with fatigue life of cortical bone (Loundagin & Edwards, 2020).

This work used a combination of high-resolution μCT imaging, mechanical testing, and finite element modelling to quantify the influence of microstructure on the fatigue behaviour of equine subchondral bone, while previous work relied only on mechanical testing and high-resolution imaging (Martig et al., 2020). Although mechanical measurements such as normalized stress and elastic modulus have been shown to correlate with fatigue life (Carter et al., 1981b; Loundagin et al., 2020), finite element models quantifying stressed volume are able to help us develop a more mechanistic understanding of the failure process. For instance, given that the elastic modulus of cortical and trabecular bone is largely driven by the volume of bone tissue present (Maquer et al., 2015; Schaffler & Burr, 1988), normalizing stress by the initial modulus accounts for the effect of lower bone volume fraction, which essentially decreases the effective cross-sectional area; however, it is somewhat limited in that does not consider how stress is

distributed throughout the sample. Conversely, a measure of stressed volume determined from finite element modelling considers the stress concentrations associated with the vascular network and quantifies the stress distribution by measuring the volume of bone subjected to elevated stress, which dictates the likelihood of encountering and propagating pre-existing microcracks. Therefore, the finite element modelling employed in this study allowed us to develop a more fundamental understanding of the failure process in equine subchondral bone.

4.3 Limitations

While this work had many strengths and was able to provide novel contributions to the field of research, this work also has a number of limitations that should be considered for future work. During the machining process, cutting may have introduced imperfections into the samples, particularly at the surface. Additionally, although polishing the samples made the surfaces appear visually planoparallel, a slightly uneven contact surface with the upper platen may still have been present which could have impacted the loading environment. However, the tuning protocol helped ensure that the sample was properly seated within the lower platen and samples often exhibited an oblique fracture pattern. The latter, indicating failure along the direction of maximum shear stress associated with pure compression.

In the μCT protocol, samples were imaged with an isotropic voxel size of 6 μm. Although scanning at this resolution resulted in some microstructural features not being captured, previous work has shown that canals less than 50 μm in diameter did not significantly influence fatigue life measurements (Loundagin & Edwards, 2020). While current equine imaging technology can achieve sub-millimetre resolution, detecting all the microstructural features described throughout this research is not currently clinically feasible. However, high-resolution peripheral quantitative computed tomography (HR-pQCT) can scan with a voxel resolution of 82 μm and has been shown

to accurately detect pores larger than 140 μm (Jorgenson et al., 2015). Therefore, current imaging technology may give valuable insights regarding larger pores, which may be most detrimental to fatigue resistance given that they would subject a larger volume of material to elevated stress.

During mechanical testing, samples were immersed in PBS at room temperature. Several studies have investigated the effects of different testing parameters on the fatigue life of cortical bone, including temperature and hydration (Carter & Hayes, 1976; Nyman et al., 2006). Since dehydration has been associated with decreased strength and toughness, samples were rehydrated prior to testing and immersed in PBS during the testing protocol. Regarding temperature, existing work has shown that fatigue life decreased by less than an order of magnitude as temperature increased from 21°C to 45°C. While logistical reasons prevented testing from taking place at 37°C, testing conditions were consistent among all samples, which resulted in systematic error. Therefore, the temperature likely did not influence the relationships seen among variables.

Biomechanical testing was conducted at a single load level due to the number of samples collected for the study. While the horses used in this study represented a variety of breeds, ages, and sex, a single load level was chosen to be able to investigate the influence of these variables without having to account for a load effect. This also maximizes our statistical power because samples were not allocated to multiple loading groups. Moving forward, more samples may be used to investigate the effect of loading amplitude.

The mechanical properties obtained from testing were subject to experimental error. Consequently, in the analysis, the measure of normalized stress was susceptible to experimental artifacts from the mechanical testing given that it required an initial modulus measurement. Conversely, all of the microstructural measurements and the stressed volume measure from the

finite element model were only dependent on the accuracy of the imaging, which may be less sensitive to potential artifacts.

The finite element model in this study assumed homogeneous material properties. Consequently, the model did not account for variation in mineral content distribution. Although the stressed volume output from the model reported strong correlations with fatigue life, quantifying the mineral distribution and incorporating heterogeneous material properties into the finite element model may explain more of the variation (Katsamenis et al., 2015).

The *ex vivo* testing in this study did not capture the remodelling response seen *in vivo*. Indeed, horses have been shown to respond to training programs through densification of the subchondral bone (Easton & Kawcak, 2007; Whitton et al., 2010), demonstrating that adaptation takes place in response to bouts of racing and training. The remodelling process creates resorption canals that can range from 200 – 300 μm in diameter (Bell et al., 1999; Cooper et al., 2016; Jordan et al., 2000). These canals are considerably larger than Haversian canals and can induce significant stress concentrations. They also reduce the effective cross-sectional area of the bone, thus decreasing its load-carrying capacity. In cortical bone samples, Loundagin et al. (2020) demonstrated that a canal with a diameter of 250 μm may increase the stressed volume by more than 25% and decrease the fatigue life by several orders of magnitude. Therefore, despite the important influence of remodelling on fatigue life, these biological aspects are not captured by testing *ex vivo*.

4.4 Future Directions and Concluding Remarks

Before we are able to move towards the prevention of fatigue fracture and the development of training protocols that can reduce the incidence of injury, there are several other avenues of work that can be pursued to further our fundamental understanding of the development of subchondral bone injuries in racehorses.

At the tissue level, to predict material failure arising from a stress concentration, it is not only necessary to know the magnitude of the stress concentration, but also the volume of bone subjected to elevated stress, as this determines the ability of a microcrack to grow within the bony matrix. The theory of critical distances not only considers the peak stress, but also quantifies the stress field surrounding a stress concentration site. This theory predicts material failure will occur when the stress reaches some critical value at a critical distance from a stress concentration feature (Taylor, 1999, 2005, 2008). In practice, stress concentrations around microarchitectural features determined from finite element models can be compared to microdamage nucleation sites and crack propagation paths using a contrast agent (Landrigan et al., 2011; Leng et al., 2008). This theory has been shown to accurately predict fatigue failure for a material with a single stress concentration feature (Taylor, 1999, 2005) and it may be used to help develop a more mechanistic understanding of the fatigue process.

While the results in Chapter Three suggested that the cortical plate may play a more prominent role in the fatigue resistance of subchondral bone, the importance of the underlying trabecular bone cannot be discounted. Indeed, previous work investigating the failure behaviour of rat vertebrae found that the combined contributions of both the cortical shell and trabecular bone must be considered as compressive failure was associated with stress concentrations sites in the cortical shell that were adjacent to regions of reduced trabecular bone volume (Morton et al., 2018).

Other work has shown that failure initiates at the "weakest link" within the trabecular network. That is, using image guided failure assessment (IGFA), failure was observed to occur in regions that possessed lower trabecular bone volume fraction compared to the average bone volume fraction for the whole sample (Nazarian et al., 2006; Nazarian & Müller, 2004; Thurner et al., 2006). IGFA is a technique that can be implemented to observe damage formation and changes in bone microarchitecture under load. In the subchondral bone samples from the MCP joint, this technique may be used to visualize damage formation and investigate how the cortical plate and underlying trabecular bone interact to influence the strength of the sample.

The complexities of fatigue failure are further emphasized at the whole-bone level, where structural geometry and density distributions lead to complex stress-strain states. Existing literature has found the articulating geometry of the MCP joint to affect the likelihood of musculoskeletal injuries in racehorses, with factors such as curvature of the lateral condyle, ratio of lateral to medial condylar width, and sagittal ridge angle all reportedly contributing to fracture risk (Kawcak et al., 2009; Liley et al., 2017). While several factors contribute to the development of equine MCP joint injuries, the stress that the tissue is subjected to plays a critical role. Therefore, these changes in joint geometry likely influence the risk of musculoskeletal injuries in racehorses by altering the stress distribution at the articular surface and within the subchondral bone. Statistical shape modelling is a sophisticated technique used to quantify the average and principal modes of variation in shape, such as bone geometry, from a training set of models (Bruce et al., 2022; Liley et al., 2018). These models may then be altered by morphing the average shape along the principal modes of variation. When combined with computational techniques such as discrete element analysis (Appendix C), a computationally efficient tool for estimating intra-articular contact stress distributions (Anderson et al., 2010; Townsend et al., 2018), statistical shape

modelling can be used to investigate how changes in joint geometry alter joint contact stress distributions and the resulting fracture risk.

By combining material level testing with whole bone modelling, these future directions can help develop a more comprehensive, multiscale understanding of MCP joint injuries. Beyond understanding how these injuries develop, the ultimate goal is to be able to prevent these injuries from occurring in the first place. The aetiology of MCP joint injury is multifactorial and several factors contribute to the risk of developing one of these injuries. At the whole bone level, previous work has found the articulating geometry of the MCP joint to affect the likelihood of musculoskeletal injuries in racehorses (Kawcak et al., 2009; Liley et al., 2017). Additionally, at the microstructural scale, this research demonstrated the influence that microarchitecture can have on fracture risk. When comparing samples from the P1 and MC3, a 23% decrease in stressed volume corresponded to an increase in the likelihood of surviving 6500 cycles by 200%. This is to say that there is a myriad of factors that can influence injury risk, ranging from the microstructural scale up to the whole bone level. Given how much these factors can vary between horses, each horse will inevitably have a different risk of developing an injury.

Currently, epidemiological data exists reporting distances horses have travelled in the month prior to sustaining a fracture (Verheyen et al., 2006). However, this is a generic framework for determining an appropriate training volume to avoid injury. Furthermore, given how much variability exists between horses with regard to bone microarchitecture, it would not be appropriate to apply the same training protocol to each horse. Instead, although more costly and time consuming, subject specific training plans would be much more beneficial as they can account for microstructural differences between subjects. To accomplish this, high resolution imaging can be used to monitor changes over the course of a racing season. Currently, second-generation HR-

pQCT scanners can achieve an isotropic voxel size of 61 μm (Manske et al., 2015) and therefore may be useful in quantifying stress concentration sites and monitoring microstructural changes within the subchondral bone. Based on these observations, we may be able to identify if an injury is developing and prescribe periods of rest when necessary. Given that racehorses exhibit suppressed remodelling during periods of high intensity exercise (Holmes et al., 2014; Whitton et al., 2010), these interventions and rest periods may help delay the onset of fatigue fracture by allowing for natural remodelling to repair damage that has accumulated. This imaging can also be used to develop subject specific discrete element models, which have been shown to provide comparable contact stress predictions as the finite element method in a fraction of the time (Anderson et al., 2010; Townsend et al., 2018). These models can monitor changes in stress distribution over the course of a season and potentially be used to infer the development of an injury. Additionally, by incorporating a stochastic failure model into discrete or finite element models, the probability of fracture can be predicted. A Weibull analysis is a well-known technique in engineering used to describe variance in brittle material failure (Taylor et al., 1999; Taylor & Kuiper, 2001). By extrapolating findings from material level tests to whole bone using finite element modelling and a Weibull analysis accounting for stressed volume, previous work has been able to accurately predict fatigue fracture in human bone at time scales consistent with *in vivo* observations (Edwards et al., 2009, 2010; Haider et al., 2022). Therefore, this may be a useful technique to provide evidence-based guidelines for appropriate training strategies that not only aim to achieve optimal cardiovascular race fitness, but also create a robust skeleton that can sustain the demands placed on it over the course of a racing career.

Ultimately, a fundamental, mechanistic understanding of the development of fatigue fracture at the MCP joint is essential before we can move towards predicting these injuries and

developing training protocols to prevent them. By improving our understanding of the variance in fatigue life measurements, this research begins to help clarify the underlying mechanisms of the mechanical fatigue process and provide a basic understanding of subchondral bone injuries in the equine MCP joint. This understanding may eventually be used to inform evidence-based training strategies and rehabilitation programs to help reduce the incidence of injury in racehorses and improve outcomes when recovering from an injury. The bone markers and microstructural features identified in this research as being the most important determinants of fatigue strength may eventually be used to inform appropriate screening measures for equine bone health as more advanced imaging methods become clinically available for the equine population.

References

Anderson, D. D., Iyer, K. S., Segal, N. A., Lynch, J. A., & Brown, T. D. (2010). Implementation of Discrete Element Analysis for Subject-Specific, Population-Wide Investigations of Habitual Contact Stress Exposure. *J Appl Biomech*, *26*(2), 215–223.

Bell, K. L., Loveridge, N., Power, J., Garrahan, N., Meggitt, B. F., & Reeve, J. (1999). Regional Differences in Cortical Porosity in the Fractured Femoral Neck. *Bone*, *24*(1), 57–64.

Bruce, O. L., Baggaley, M., Welte, L., Rainbow, M. J., & Edwards, W. B. (2022). A statistical shape model of the tibia-fibula complex: sexual dimorphism and effects of age on reconstruction accuracy from anatomical landmarks. *Computer Methods in Biomechanics and Biomedical Engineering*, *25*(8), 875–886. https://doi.org/10.1080/10255842.2021.1985111

Burr, D. B., Martin, B. R., Schaffler, M. B., & Radin, E. L. (1985). Bone Remodelling in Response to In Vivo Fatigue Microdamage. *Journal of Biomechanics*, *18*(3), 189–200.

Burr, D. B., Milgrom, C., Boyd, R. D., Higgins, W. L., Robin, G., & Radin, E. L. (1990). Experimental Stress Fractures of the Tibia Biological and Mechanical Aetiology in Rabbits. In *J Bone Joint Surg [Br]* (Vol. 72).

Burr, D. B., Turner, C. H., Naick, P., Forwood, M. R., Ambrosius, W., Hasan, M. S., & Pidaparti, R. (1998). Does microdamage accumulation affect the mechanical properties of bone? In *Journal of Biomechanics* (Vol. 31).

Caler, W. E., & Carter, D. R. (1989). Bone Creep-Fatigue Damage Accumulation. *Journal of Biomechanics*, *22*(6), 625435.

Carpenter, B., Gelman, A., Hoffman, M. D., Lee, D., Goodrich, B., Betancourt, M., Brubaker, M. A., Guo, J., Li, P., & Riddell, A. (2017). Stan: A probabilistic programming language. *Journal of Statistical Software*, *76*(1). https://doi.org/10.18637/jss.v076.i01

Carter, D. R., Caler, W. E., Spengler, D. M., & Frankel, V. H. (1981a). Fatigue behavior of adult cortical bone: the influence of mean strain and strain range. *Acta Orthopaedica*, *52*(5), 481–490. https://doi.org/10.3109/17453678108992136

Carter, D. R., Caler, W. E., Spengler, D. M., & Frankel, V. H. (1981b). Uniaxial Fatigue of Human Cortical Bone. The Influence of Tissue Physical Characteristics. *Journal of Biomechanics*, *14*, 461–470.

Carter, D. R., & Hayes, W. C. (1976). Fatigue Life of Compact Bone - I Effects of Stress Amplitude, Temperature and Density. *Journal of Biomechanics*, *9*, 27.

Carter, D. R., & Hayes, W. C. (1977). Compact Bone Fatigue Damage-I. Residual Strength and Stiffness. *Journal of Biomechanics*, *10*, 325–337.

Clayton, H. M., Sha, D., Stick, J., & Elvin, N. (2007). 3D kinematics of the equine metacarpophalangeal joint at walk and trot. *Veterinary and Comparative Orthopaedics and Traumatology*, *20*, 86–91. https://doi.org/10.1160/VCOT-07-01-0011

Colgate, V. A., & Marr, C. M. (2020). Science-in-brief: Risk assessment for reducing injuries of the fetlock bones in Thoroughbred racehorses. *Equine Veterinary Journal*, *52*(4), 482–488. https://doi.org/10.1111/evj.13273

Cooper, D. M. L., Kawalilak, C. E., Harrison, K., Johnston, B. D., & Johnston, J. D. (2016). Cortical Bone Porosity: What Is It, Why Is It Important, and How Can We Detect It? In *Current Osteoporosis Reports* (Vol. 14, Issue 5, pp. 187–198). Current Medicine Group LLC 1. https://doi.org/10.1007/s11914-016-0319-y

Currey, J. (2004). Incompatible mechanical properties in compact bone. *Journal of Theoretical Biology*, *231*(4), 569–580. https://doi.org/10.1016/j.jtbi.2004.07.013

Currey, J. D., Brear, K., & Zioupos, P. (1996). The effects of ageing and changes in mineral content in degrading the toughness of human femora. *Journal of Biomechanics*, *29*(2), 257–260.

Davis, T., Healy, D., Bubeck, A., & Walker, R. (2017). Stress concentrations around voids in three dimensions: The roots of failure. *Journal of Structural Geology*, *102*, 193–207. https://doi.org/10.1016/j.jsg.2017.07.013

Doube, M., Klosowski, M. M., Arganda-Carreras, I., Cordelières, F. P., Dougherty, R. P., Jackson, J. S., Schmid, B., Hutchinson, J. R., & Shefelbine, S. J. (2010). BoneJ: Free and extensible bone image analysis in ImageJ. *Bone*, *47*(6), 1076–1079. https://doi.org/10.1016/j.bone.2010.08.023

Easton, K. L., & Kawcak, C. E. (2007). Evaluation of increased subchondral bone density in areas of contact in the metacarpophalangeal joint during joint loading in horses. *American Journal of Veterinary Research*, *68*(8), 816–821.

Edwards, W. B., Taylor, D., Rudolphi, T. J., Gillette, J. C., & Derrick, T. R. (2009). Effects of Stride Length and Running Mileage on a Probabilistic Stress Fracture Model. *Medicine and Science in Sports and Exercise*, *41*(12), 2177–2184.

Edwards, W. B., Taylor, D., Rudolphi, T. J., Gillette, J. C., & Derrick, T. R. (2010). Effects of running speed on a probabilistic stress fracture model. *Clinical Biomechanics*, *25*(4), 372–377. https://doi.org/10.1016/j.clinbiomech.2010.01.001

Ellis, D. R. (1994). Some observations on condylar fractures of the third metacarpus and third metatarsus in young Thoroughbreds. *Equine Veterinary Journal*, *26*(3), 178–183.

Ethier, C. R., & Simmons, C. A. (2007). *Introductory Biomechanics From Cells to Organisms*. Cambridge University Press, New York.

Fatihhi, S. J., Harun, M. N., Abdul Kadir, M. R., Abdullah, J., Kamarul, T., Öchsner, A., & Syahrom, A. (2015). Uniaxial and Multiaxial Fatigue Life Prediction of the Trabecular

Bone Based on Physiological Loading: A Comparative Study. *Annals of Biomedical Engineering*, *43*(10), 2487–2502. https://doi.org/10.1007/s10439-015-1305-8

Gelman, A., & Rubin, D. B. (1992). Inference from Iterative Simulation Using Multiple Sequences. *Statistical Science*, *7*(4), 457–511.

Graham, R. H., Raines, M., Swift, K. G., & Gui, L. (2005). Prediction of stress concentrations associated with interacting stress-raisers within aircraft design: Methodology development and application. *Proceedings of the Institution of Mechanical Engineers, Part G: Journal of Aerospace Engineering*, *219*(3), 193–204. https://doi.org/10.1243/095441005X30225

Haider, I. T., Loundagin, L. L., Sawatsky, A., Kostenuik, P. J., Boyd, S. K., & Edwards, W. B. (2023). Twelve Months of Denosumab and/or Alendronate Is Associated With Improved Bone Fatigue Life, Microarchitecture, and Density in Ovariectomized Cynomolgus Monkeys. *Journal of Bone and Mineral Research*, *38*(3), 403–413. https://doi.org/10.1002/jbmr.4781

Haider, I. T., Pohl, A. J., & Edwards, W. B. (2022). The probability of whole-bone fatigue fracture can be accurately predicted using specimen-specific finite element analysis incorporating a stochastic failure model. *Journal of Biomechanics*, *143*. https://doi.org/10.1016/j.jbiomech.2022.111273

Harrison, S. M., Chris Whitton, R., Kawcak, C. E., Stover, S. M., & Pandy, M. G. (2014). Evaluation of a subject-specific finite-element model of the equine metacarpophalangeal joint under physiological load. *Journal of Biomechanics*, *47*(1), 65–73. https://doi.org/10.1016/J.JBIOMECH.2013.10.001

Harrison, S. M., Whitton, R. C., Kawcak, C. E., Stover, S. M., & Pandy, M. G. (2010). Relationship between muscle forces, joint loading and utilization of elastic strain energy in equine locomotion. *The Journal of Experimental Biology*, *213*, 3998–4009. https://doi.org/10.1242/jeb.044545

Hernandez, C. J., Gupta, A., & Keaveny, T. M. (2006). A biomechanical analysis of the effects of resorption cavities on cancellous bone strength. *Journal of Bone and Mineral Research*, *21*(8), 1248–1255. https://doi.org/10.1359/jbmr.060514

Hoey, D., & Taylor, D. (2009). Quantitative analysis of the effect of porosity on the fatigue strength of bone cement. *Acta Biomaterialia*, *5*(2), 719–726. https://doi.org/10.1016/j.actbio.2008.08.024

Holmes, J. M., Mirams, M., Mackie, E. J., & Whitton, R. C. (2014). Thoroughbred horses in race training have lower levels of subchondral bone remodelling in highly loaded regions of the distal metacarpus compared to horses resting from training. *The Veterinary Journal*, *202*(3), 443–447. https://doi.org/10.1016/J.TVJL.2014.09.010

Hougaard, P. (2000). *Analysis of Multivariate Survival Data*. Statistics for Biology and Health. Springer New York.

Ibrahim, J. G., Chen, M.-H., & Sinha, D. (2001). *Bayesian Survival Analysis*. Springer Series in Statistics. Springer New York.

Johnson, B. J., Stover, S. M., Daft, B. M., Kinde, H., Read, D. H., Barr, B. C., Anderson, M., Moore, J., Woods, L., Stoltz, J., & Blanchard, P. (1994). Causes of death in racehorses over a 2 year period. *Equine Veterinary Journal*, *26*(4), 327–330.

Jordan, G. R., Loveridge, N., Bell, K. L., Power, J., Rushton, N., & Reeve, J. (2000). Spatial Clustering of Remodeling Osteons in the Femoral Neck Cortex: A Cause of Weakness in Hip Fracture? *Bone*, *26*(3), 305–313.

Jorgenson, B. L., Buie, H. R., McErlain, D. D., Sandino, C., & Boyd, S. K. (2015). A comparison of methods for in vivo assessment of cortical porosity in the human appendicular skeleton. *Bone*, *73*, 167–175. https://doi.org/10.1016/j.bone.2014.11.023

Katsamenis, O. L., Jenkins, T., & Thurner, P. J. (2015). Toughness and damage susceptibility in human cortical bone is proportional to mechanical inhomogeneity at the osteonal-level. *Bone*, *76*, 158–168. https://doi.org/10.1016/j.bone.2015.03.020

Kawcak, C., McIlwraith, C., Parkin, T., Easton, K., & Zimmerman, C. (2009). The Effects of Third Metacarpal Geometry on the Incidence of Condylar Fractures in Thoroughbred Racehorses. *Osteoarthritis and Cartilage*, *17*, S237–S238. https://doi.org/10.1016/s1063-4584(09)60466-0

Keaveny, T. M., Morgan, E. F., Niebur, G. L., & Yeh, O. C. (2001). Biomechanics of Trabecular Bone. *Annual Review of Biomedical Engineering*, *3*, 307–333.

Landrigan, M. D., Li, J., Turnbull, T. L., Burr, D. B., Niebur, G. L., & Roeder, R. K. (2011). Contrast-enhanced micro-computed tomography of fatigue microdamage accumulation in human cortical bone. *Bone*, *48*(3), 443–450. https://doi.org/10.1016/j.bone.2010.10.160

Launey, M. E., Buehler, M. J., & Ritchie, R. O. (2010). On the mechanistic origins of toughness in bone. *Annual Review of Materials Research*, *40*, 25–53. https://doi.org/10.1146/annurev-matsci-070909-104427

Lee, H., Kirkland, W. G., Whitmore, R. N., Theis, K. M., Young, H. E., Richardson, A. J., Jackson, R. L., & Hanson, R. R. (2014). Comparison of equine articular cartilage thickness in various joints. *Connective Tissue Research*, *55*(5–6), 339–347. https://doi.org/10.3109/03008207.2014.949698

Leng, H., Wang, X., Ross, R. D., Niebur, G. L., & Roeder, R. K. (2008). Micro-computed tomography of fatigue microdamage in cortical bone using a barium sulfate contrast agent. *Journal of the Mechanical Behavior of Biomedical Materials*, *1*(1), 68–75. https://doi.org/10.1016/j.jmbbm.2007.06.002

Li, G., Yin, J., Gao, J., Cheng, T. S., Pavlos, N. J., Zhang, C., & Zheng, M. H. (2013). Subchondral bone in osteoarthritis: insight into risk factors and microstructural changes. *Arthritis Research and Therapy*, *15*(223). http://arthritis-research.com/content/15/6/223

Liley, H., Davies, H., Firth, E., Besier, T., & Fernandez, J. (2017). The effect of the sagittal ridge angle on cartilage stress in the equine metacarpo-phalangeal (fetlock) joint. *Computer Methods in Biomechanics and Biomedical Engineering*, *20*(10), 1140–1149. https://doi.org/10.1080/10255842.2017.1339795

Liley, H., Zhang, J., Firth, E. C., Fernandez, J. W., & Besier, T. F. (2018). Statistical modeling of the equine third metacarpal bone incorporating morphology and bone mineral density. *PLoS ONE*, *13*(6). https://doi.org/10.1371/journal.pone.0194406

Loundagin, L. L., & Edwards, W. B. (2020). Stressed volume around vascular canals explains compressive fatigue life variation of secondary osteonal bone but not plexiform bone. *Journal of the Mechanical Behavior of Biomedical Materials*, *111*. https://doi.org/10.1016/j.jmbbm.2020.104002

Loundagin, L. L., Haider, I. T., Cooper, D. M. L., & Edwards, W. B. (2020). Association between intracortical microarchitecture and the compressive fatigue life of human bone: A pilot study. *Bone Reports*, *12*. https://doi.org/10.1016/j.bonr.2020.100254

Loundagin, L. L., Pohl, A. J., & Edwards, W. B. (2021). Stressed volume estimated by finite element analysis predicts the fatigue life of human cortical bone: The role of vascular canals as stress concentrators. *Bone*, *143*. https://doi.org/10.1016/j.bone.2020.115647

Loundagin, L. L., Schmidt, T. A., & Brent Edwards, W. (2018). Mechanical Fatigue of Bovine Cortical Bone Using Ground Reaction Force Waveforms in Running. *Journal of Biomechanical Engineering*, *140*(3). https://doi.org/10.1115/1.4038288

Manske, S. L., Zhu, Y., Sandino, C., & Boyd, S. K. (2015). Human trabecular bone microarchitecture can be assessed independently of density with second generation HR-pQCT. *Bone*, *79*, 213–221. https://doi.org/10.1016/j.bone.2015.06.006

Maquer, G., Musy, S. N., Wandel, J., Gross, T., & Zysset, P. K. (2015). Bone volume fraction and fabric anisotropy are better determinants of trabecular bone stiffness than other morphological variables. *Journal of Bone and Mineral Research*, *30*(6), 1000–1008. https://doi.org/10.1002/jbmr.2437

Martig, S., Chen, W., Lee, P. V. S., & Whitton, R. C. (2014). Bone fatigue and its implications for injuries in racehorses. *Equine Veterinary Journal*, *46*, 408–415. https://doi.org/10.1111/evj.12241

Martig, S., Hitchens, P. L., Lee, P. V. S., & Whitton, R. C. (2020). The relationship between microstructure, stiffness and compressive fatigue life of equine subchondral bone. *Journal of the Mechanical Behavior of Biomedical Materials*, *101*, 103439. https://doi.org/10.1016/J.JMBBM.2019.103439

Martig, S., Hitchens, P. L., Stevenson, M. A., & Whitton, R. C. (2018). Subchondral bone morphology in the metacarpus of racehorses in training changes with distance from the articular surface but not with age. *Journal of Anatomy*, *232*, 919–930. https://doi.org/10.1111/joa.12794

Martig, S., Lee, P. V. S., Anderson, G. A., & Whitton, R. C. (2013). Compressive fatigue life of subchondral bone of the metacarpal condyle in thoroughbred racehorses. *Bone*, *57*(2), 392–398. https://doi.org/10.1016/J.BONE.2013.09.006

McCarty, C. A., Thomason, J. J., Gordon, K. D., Burkhart, T. A., Milner, J. S., & Holdsworth, D. W. (2016). Finite-Element Analysis of Bone Stresses on Primary Impact in a Large-Animal Model: The Distal End of the Equine Third Metacarpal. *PLoS ONE*, *11*(7), 159541. https://doi.org/10.1371/journal.pone.0159541

McIlwraith, C. W., Frisbie, D. D., Kawcak, C., & van Weeren, R. (2015). *Joint Disease in the Horse* (2nd Edition). Elsevier Inc.

McNamara, L. M., Van Der Linden, J. C., Weinans, H., & Prendergast, P. J. (2006). Stress-concentrating effect of resorption lacunae in trabecular bone. *Journal of Biomechanics*, *39*(4), 734–741. https://doi.org/10.1016/j.jbiomech.2004.12.027

Merritt, J. S., Davies, H. M. S., Burvill, C., & Pandy, M. G. (2008). Influence of muscle-tendon wrapping on calculations of joint reaction forces in the equine distal forelimb. *Journal of Biomedicine and Biotechnology*, *2008*(1). https://doi.org/10.1155/2008/165730

Mori, S., & Burr, D. B. (1993). Increased Intracortical Remodeling Following Fatigue Damage. *Bone*, *14*, 103–109.

Morrice-West, A. V., Hitchens, P. L., Walmsley, E. A., Stevenson, M. A., Wong, A. S. M., & Whitton, R. C. (2021). Variation in GPS and accelerometer recorded velocity and stride parameters of galloping Thoroughbred horses. *Equine Veterinary Journal*, *53*(5), 1063–1074. https://doi.org/10.1111/evj.13370

Morton, J. J., Bennison, M., Lievers, W. B., Waldman, S. D., & Pilkey, A. K. (2018). Failure behaviour of rat vertebrae determined through simultaneous compression testing and micro-CT imaging. *Journal of the Mechanical Behavior of Biomedical Materials*, *79*, 73–82. https://doi.org/10.1016/j.jmbbm.2017.11.021

Mullins, L. P., Mcgarry, J. P., Bruzzi, M. S., & Mchugh, P. E. (2007). Micromechanical modelling of cortical bone. *Computer Methods in Biomechanics and Biomedical Engineering*, *10*(3), 159–169. https://doi.org/10.1080/10255840601110802

Musy, S. N., Maquer, G., Panyasantisuk, J., Wandel, J., & Zysset, P. K. (2017). Not only stiffness, but also yield strength of the trabecular structure determined by non-linear μFE is best predicted by bone volume fraction and fabric tensor. *Journal of the Mechanical Behavior of Biomedical Materials*, *65*, 808–813. https://doi.org/10.1016/j.jmbbm.2016.10.004

Nalla, R. K., Kinney, J. H., & Ritchie, R. O. (2003). Mechanistic fracture criteria for the failure of human cortical bone. In *Nature Materials* (Vol. 2, Issue 3, pp. 164–168). European Association for Cardio-Thoracic Surgery. https://doi.org/10.1038/nmat832

Nalla, R. K., Stölken, J. S., Kinney, J. H., & Ritchie, R. O. (2005). Fracture in human cortical bone: Local fracture criteria and toughening mechanisms. *Journal of Biomechanics*, *38*(7), 1517–1525. https://doi.org/10.1016/j.jbiomech.2004.07.010

Nazarian, A., & Müller, R. (2004). Time-lapsed microstructural imaging of bone failure behavior. *Journal of Biomechanics*, *37*(1), 55–65. https://doi.org/10.1016/S0021-9290(03)00254-9

Nazarian, A., Stauber, M., Zurakowski, D., Snyder, B. D., & Müller, R. (2006). The interaction of microstructure and volume fraction in predicting failure in cancellous bone. *Bone*, *39*(6), 1196–1202. https://doi.org/10.1016/j.bone.2006.06.013

Nicolella, D. P., Bonewald, L. F., Moravits, D. E., & Lankford, J. (2005). Measurement of microstructural strain in cortical bone. *European Journal of Morphology*, *42*, 23–29.

Nixon, A. J. (2020). *Equine Fracture Repair Second Edition* (Second). John Wiley & Sons, Inc. http://www.wiley.com/go/permissions.

Nunamaker, D. M., Butterweck, D. M., & Provost, M. T. (1989). Some Geometric Properties of the Third Metacarpal Bone: A Comparison Between the Thoroughbred and Standardbred Racehorse. *Journal of Biomechanics*, *22*(2), 129–134.

Nyman, J. S., Roy, A., Shen, X., Acuna, R. L., Tyler, J. H., & Wang, X. (2006). The influence of water removal on the strength and toughness of cortical bone. *Journal of Biomechanics*, *39*(5), 931–938. https://doi.org/10.1016/j.jbiomech.2005.01.012

O'Brien, F. J., Taylor, D., & Lee, T. C. (2003). Microcrack accumulation at different intervals during fatigue testing of compact bone. *Journal of Biomechanics*, *36*(7), 973–980. https://doi.org/10.1016/S0021-9290(03)00066-6

O'Brien, F. J., Taylor, D., & Lee, T. C. (2005). The effect of bone microstructure on the initiation and growth of microcracks. *Journal of Orthopaedic Research*, *23*(2), 475–480. https://doi.org/10.1016/J.ORTHRES.2004.08.005

Radtke, C. L., Danova, N. A., Scollay, M. C., Santschi, E. M., Markel, M. D., Da Costa Gómez, T., & Muir, P. (2003). Macroscopic changes in the distal ends of the third metacarpal and metatarsal bones of Thoroughbred racehorses with condylar fractures. *American Journal of Veterinary Research*, *64*(9), 1110–1116.

Rapillard, L., Charlebois, M., & Zysset, P. K. (2006). Compressive fatigue behavior of human vertebral trabecular bone. *Journal of Biomechanics*, *39*(11), 2133–2139. https://doi.org/10.1016/j.jbiomech.2005.04.033

Riegel, R. J., & Hakola, S. E. (1996). *Illustrated Atlas of Clinical Equine Anatomy and Common Disorders of the Horse* (Vol. 1). Equistar Publications, Marysville, OH.

Riggs, C. M. (1999). Aetiopathogenesis of parasagittal fractures of the distal condyles of the third metacarpal and third metatarsal bones - Review of the literature. *Equine Veterinary Journal*, *31*(2), 116–120. https://doi.org/10.1111/j.2042-3306.1999.tb03803.x

Riggs, C. M. (2002). Fractures - A preventable hazard of racing thoroughbreds? *Veterinary Journal*, *163*(1), 19–29. https://doi.org/10.1053/tvjl.2001.0610

Riggs, C. M., & Boyde, A. (1999). Effect of exercise on bone density in distal regions of the equine third metacarpal bone in 2-year-old thoroughbreds. *Equine Veterinary Journal. Supplement*, *30*, 555–560. https://doi.org/10.1111/j.2042-3306.1999.tb05283.x

Riggs, C. M., Whitehouse, G. H., & Boyde, A. (1999a). Pathology of the distal condyles of the third metacarpal and third metatarsal bones of the horse. *Equine Veterinary Journal*, *31*(2), 140–148. https://doi.org/10.1111/j.2042-3306.1999.tb03807.x

Riggs, C. M., Whitehouse, G. H., & Boyde, A. (1999b). Structural variation of the distal condyles of the third metacarpal and third metatarsal bones in the horse. *Equine Veterinary Journal*, *31*(2), 130–139.

Rosanowski, S. M., Chang, Y. M., Stirk, A. J., & Verheyen, K. L. P. (2017). Descriptive epidemiology of veterinary events in flat racing Thoroughbreds in Great Britain (2000 to 2013). *Equine Veterinary Journal*, *49*(3), 275–281. https://doi.org/10.1111/evj.12592

Rosanowski, S. M., Chang, Y. M., Stirk, A. J., & Verheyen, K. L. P. (2019). Epidemiology of race-day distal limb fracture in flat racing Thoroughbreds in Great Britain (2000–2013). *Equine Veterinary Journal*, *51*(1), 83–89. https://doi.org/10.1111/evj.12968

Rubio-Martínez, L. M., Cruz, A. M., Gordon, K., & Hurtig, M. B. (2008). Mechanical properties of subchondral bone in the distal aspect of third metacarpal bones from Thoroughbred racehorses. *American Journal of Veterinary Research*, *69*(11), 1423–1433. https://doi.org/10.2460/ajvr.69.11.1423

Santschi, E. M. (2008). Articular Fetlock Injuries in Exercising Horses. In *Veterinary Clinics of North America - Equine Practice* (Vol. 24, Issue 1, pp. 117–132). https://doi.org/10.1016/j.cveq.2007.11.011

Schaffler, M. B., & Burr, D. B. (1988). Stiffness of Compact Bone: Effects of Porosity and Density. *Journal of Biomechanics*, *21*(1), 13–16.

Schindelin, J., Arganda-Carreras, I., Frise, E., Kaynig, V., Longair, M., Pietzsch, T., Preibisch, S., Rueden, C., Saalfeld, S., Schmid, B., Tinevez, J. Y., White, D. J., Hartenstein, V., Eliceiri, K., Tomancak, P., & Cardona, A. (2012). Fiji: An open-source platform for biological-image analysis. In *Nature Methods* (Vol. 9, Issue 7, pp. 676–682). https://doi.org/10.1038/nmeth.2019

Shaktivesh, S., Malekipour, F., Whitton, R. C., Hitchens, P. L., & Lee, P. V. (2020). Fatigue behavior of subchondral bone under simulated physiological loads of equine athletic training. *Journal of the Mechanical Behavior of Biomedical Materials*, *110*, 103920. https://doi.org/10.1016/J.JMBBM.2020.103920

Stepnik, M. W., Radtke, C. L., Scollay, M. C., Oshel, P. E., Albrecht, R. M., Santschi, E. M., Markel, M. D., & Muir, P. (2004). Scanning electron microscopic examination of third metacarpal/third metatarsal bone failure surfaces in Thoroughbred racehorses with condylar

fracture. *Veterinary Surgery*, *33*(1), 2–10. https://doi.org/10.1111/j.1532-950x.2004.04007.x

Suresh, S. (1998). *Fatigue of Materials*. Cambridge University Press.

Takahashi, Y., Takahashi, T., Mukai, K., & Ohmura, H. (2021). Effects of Fatigue on Stride Parameters in Thoroughbred Racehorses During Races. *Journal of Equine Veterinary Science*, *101*. https://doi.org/10.1016/j.jevs.2021.103447

Taylor, D. (1998). Fatigue of bone and bones: An analysis based on stressed volume. *Journal of Orthopaedic Research*, *16*(2), 163–169. https://doi.org/10.1002/jor.1100160203

Taylor, D. (1999). Geometrical effects in fatigue: a unifying theoretical model. In *International Journal of Fatigue* (Vol. 21).

Taylor, D. (2005). Analysis of fatigue failures in components using the theory of critical distances. *Engineering Failure Analysis*, *12*(6 SPEC. ISS.), 906–914. https://doi.org/10.1016/j.engfailanal.2004.12.007

Taylor, D. (2008). The theory of critical distances. *Engineering Fracture Mechanics*, *75*(7), 1696–1705. https://doi.org/10.1016/j.engfracmech.2007.04.007

Taylor, D., & Kuiper, J. H. (2001). The prediction of stress fractures using a "stressed volume" concept. *Journal of Orthopaedic Research*, *19*(5), 919–926. https://doi.org/10.1016/S0736-0266(01)00009-2

Taylor, D., O'Brien, F., Prina-Mello, A., Ryan, C., O'Reilly, P., & Lee, Clive. T. (1999). Compression data on bovine bone confirms that a "stressed volume" principle explains the variability of fatigue strength results. *Journal of Biomechanics*, *32*, 1199–1203.

Thurner, P. J., Wyss, P., Voide, R., Stauber, M., Stampanoni, M., Sennhauser, U., & Müller, R. (2006). Time-lapsed investigation of three-dimensional failure and damage accumulation in trabecular bone using synchrotron light. *Bone*, *39*(2), 289–299. https://doi.org/10.1016/j.bone.2006.01.147

Topoliński, T., & Mazurkiewicz, A. (2012). Relationship Between Fatigue Life and Structure of Human Trabecular Bone. *18th International Conference Engineering Mechanics*, 1419–1423.

Torres, A. M., Trikanad, A. A., Aubin, C. A., Lambers, M., Luna, M., Rimnac, C. M., Zavattieri, P., & Hernandez, C. J. (2019). Bone-inspired microarchitectures achieve enhanced fatigue life. *The Proceedings of the National Academy of Sciences*, *116*(49), 24457–24462. https://doi.org/10.1073/pnas.1905814116/-/DCSupplemental

Townsend, K. C., Thomas-Aitken, H. D., Rudert, M. J., Kern, A. M., Willey, M. C., Anderson, D. D., & Goetz, J. E. (2018). Discrete element analysis is a valid method for computing joint contact stress in the hip before and after acetabular fracture. *Journal of Biomechanics*, *67*, 9–17. https://doi.org/10.1016/j.jbiomech.2017.11.014

Van Der Harst, M. R., Van Lest, C. H. A. D. E., Degroot, J., Kiers, G. H., Brama, P. A. J., & Van Weeren, P. R. (2005). Study of cartilage and bone layers of the bearing surface of the equine metacarpophalangeal joint relative to different timescales of maturation. *Equine Veterinary Journal*, *37*(3), 200–206. https://doi.org/10.2746/0425164054530678

Vaughan, T. J., Verbruggen, S. W., & Mcnamara, L. M. (2013). Are all osteocytes equal? Multiscale modelling of cortical bone to characterise the mechanical stimulation of osteocytes. *International Journal for Numerical Methods in Biomedical Engineering*, *29*(12), 1361–1372. https://doi.org/10.1002/cnm.2578

Vehtari, A., Gelman, A., & Gabry, J. (2017). Practical Bayesian model evaluation using leave-one-out cross-validation and WAIC. *Statistics and Computing*, *27*(5), 1413–1432. https://doi.org/10.1007/s11222-016-9696-4

Verbruggen, S. W., Vaughan, T. J., & McNamara, L. M. (2012). Strain amplification in bone mechanobiology: A computational investigation of the in vivo mechanics of osteocytes. *Journal of the Royal Society Interface*, *9*(75), 2735–2744. https://doi.org/10.1098/rsif.2012.0286

Verheyen, K., Price, J., Lanyon, L., & Wood, J. (2006). Exercise distance and speed affect the risk of fracture in racehorses. *Bone*, *39*(6), 1322–1330. https://doi.org/10.1016/j.bone.2006.05.025

Wang, X., Bank, R. A., TeKoppele, J. M., & Mauli Agrawal, C. (2001). The role of collagen in determining bone mechanical properties. *Journal of Orthopaedic Research*, *19*(6), 1021–1026. https://doi.org/10.1016/S0736-0266(01)00047-X

Whitton, R. C., Trope, G. D., Ghasem-Zadeh, A., Anderson, G. A., Parkin, T. D. H., Mackie, E. J., & Seeman, E. (2010). Third metacarpal condylar fatigue fractures in equine athletes occur within previously modelled subchondral bone. *Bone*, *47*(4), 826–831. https://doi.org/10.1016/J.BONE.2010.07.019

Yeni, Y. N., & Norman, T. L. (2000). Calculation of porosity and osteonal cement line effects on the effective fracture toughness of cortical bone in longitudinal crack growth. *Journal of Biomedical Materials Research*, *51*(3), 504–509. https://doi.org/10.1002/1097-4636(20000905)51:3<504::AID-JBM27>3.0.CO;2-I

Zhu, X., Chan, Y. T., Yung, P. S. H., Tuan, R. S., & Jiang, Y. (2021). Subchondral Bone Remodeling: A Therapeutic Target for Osteoarthritis. In *Frontiers in Cell and Developmental Biology* (Vol. 8). Frontiers Media S.A. https://doi.org/10.3389/fcell.2020.607764

Zimmermann, E. A., & Ritchie, R. O. (2015). Bone as a Structural Material. In *Advanced Healthcare Materials* (Vol. 4, Issue 9, pp. 1287–1304). Wiley-VCH Verlag. https://doi.org/10.1002/adhm.201500070

Zioupos, P., Currey, J. D., & Casinos, A. (2001). Tensile fatigue in bone: Are cycles-, or time to failure, or both, important? *Journal of Theoretical Biology*, *210*(3), 389–399. https://doi.org/10.1006/jtbi.2001.2316

Zioupos, P., Gresle, M., & Winwood, K. (2008). Fatigue strength of human cortical bone: Age, physical, and material heterogeneity effects. *Journal of Biomedical Materials Research - Part A*, *86*(3), 627–636. https://doi.org/10.1002/jbm.a.31576

Appendix A

Fatigue Behaviour of Equine Subchondral Bone from the Metacarpophalangeal Joint at Two Different Loading Frequencies

The biomechanical testing in this study was conducted at a loading frequency of 2 Hz. This frequency was chosen to mimic physiological loading and to facilitate comparison with existing literature (Martig et al., 2013, 2020; Morrice-West et al., 2021; Takahashi et al., 2021). However, other work has demonstrated that bone may exhibit different fatigue life behaviour depending on the frequency of loading. Zioupus et al. (2001) found that the number of cycles to failure was highly dependant on the loading frequency when testing samples in zero tension at 0.5 Hz and 5 Hz. Similarly, Loundagin et al. (2018) found a difference in the number of cycles to failure by testing samples in zero compression at 3 Hz and 9 Hz. Therefore, we first quantified the fatigue behaviour of equine subchondral bone from the metacarpophalangeal (MCP) joint at two different loading frequencies.

Samples were prepared and tested using the same methodology described in the paper. Briefly, 9 forelimbs were harvested and cylindrical bone samples measuring 6.7 mm in diameter were extracted from the medial and lateral condyles of the third metacarpal (MC3) and proximal phalanx (P1) using a drill press, yielding 4 samples per limb. The demographic information of the horses was unknown. Samples were cut to a length of 8 mm and the cartilage was removed using a bandsaw. The samples were polished to ensure surfaces were planoparallel. Specimens were then wrapped in gauze soaked in phosphate buffered saline (PBS) and stored in a -30°C freezer. Prior to testing, samples were thawed and rehydrated in PBS at room temperature for two hours. The proximal (i.e., trabecular) 2 mm of each sample was potted with bone cement into a lower platen. The articular surface was left unconstrained in contact with a flat upper platen fixed to a 10 kN

load cell in line with the actuator of the materials testing machine (ElectroPulse E10000, Instron, Norwood, MA, USA). Samples were tuned to a stress of 23 MPa (20% of yield strength) and fatigue life was assessed by cyclically loading samples between 0.8 and 70 MPa of compression under load control at a frequency of 2 Hz and 0.2 Hz. Samples were allocated to each group based on apparent density. Normalized stress was calculated by dividing the applied stress by the initial modulus and failure was defined using a stiffness criterion.

A plot of normalized stress and fatigue life is shown in Figure A-1. The slope and intercept of each regression line is reported in Table A-1. Based on the 95% confidence intervals, it is evident that there is no significant difference in the cycles to failure for samples from the MCP joint when loaded and 2 Hz verses 0.2 Hz.

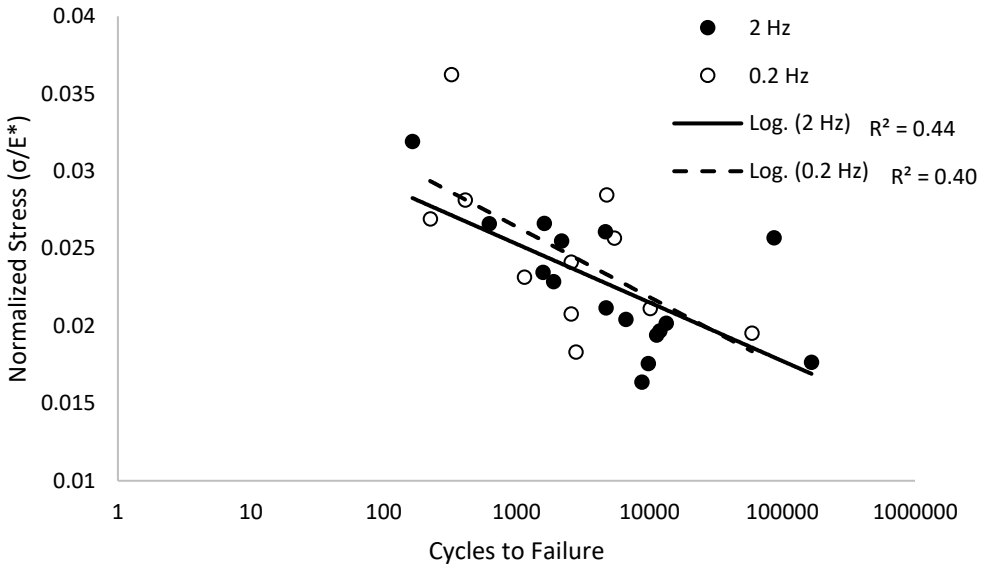

Figure A-1: Plot of normalized stress and cycles to failure for samples from the MCP joint tested at 2 Hz and 0.2 Hz

Table A-1: Slope and intercept along with the 95% confidence interval for the 2 Hz and 0.2 Hz regression lines

	2 Hz	0.2 Hz
Slope (95% CI)	-0.0038 (-0.0062, -0.0013)	-0.0045 (-0.0088, -0.0003)
Intercept (95% CI)	0.037 (0.027, 0.046)	0.04 (0.026, 0.055)

Appendix B

Details of Statistical Analysis

A Bayesian, frailty model with Weibull baseline hazard was developed (Hougaard, 2000; Ibrahim et al., 2001). The distribution of failure times T_{ij} for $j = 1, \ldots B_i$ cylindrical samples from $i = 1, \ldots n$ horses are assumed to be well described by a Weibull distribution with shape $\alpha > 0$ and varying scale $\sigma_{ij} > 0$. That is:

$$p(T_{ij}|\alpha, \sigma_{ij}) = \frac{\alpha}{\sigma_{ij}} e^{-\frac{T_{ij}}{\sigma_{ij}}\alpha}$$

with sample specific scale parameters σ_{ij} given by:

$$\sigma_{ij} = \omega_i e^{-\frac{\mu + x_{ij}^T \beta}{\alpha}}$$

Here $\boldsymbol{x_{ij}}$ denotes a vector of sample specific covariates which includes an indicator for the bone (MC3 or PC1), the microarchitectural parameter of interest, and an interaction between bone and architectural parameter. The corresponding vector of effects β describes increases or decreases in expected failure time given unit change in the associated co-variate with μ describing the average failure time across all samples.

Horse specific frailty terms $\omega_i > 0$ act multiplicatively on the resulting conditional hazard. These are assumed to follow a gamma distribution with expectation equal to one:

$$\omega_i \sim \text{Gamma}\ (\xi, \xi)$$

where $\xi > 0$. As a result, if $\omega_i > 1$ then samples from horse i are at greater risk of failure.

A weekly regularizing multivariate normal prior with large variance and no correlation was assumed for the effect of bone, microarchitecture and any possible interaction:

$$\beta \sim \text{Multivariate} - \text{Normal}\ (\mathbf{0}, 100^2 \boldsymbol{I}_3)$$

Relatively diffuse priors were used for the shape of the baseline hazard (α) and the log of expected failure time (μ):

$$\alpha \sim \text{Normal}\ (0, 10)$$

$$\mu \sim \text{Normal}\ (0, 100)$$

Similarly, a diffuse, gamma prior was assumed for hyperparameter ξ:

$$\xi \sim \text{Gamma}\ (1, 1)$$

To perform inference, 8000 samples from the posterior distribution were obtained via four independent chains of Hamiltonian Monte Carlo sampling utilizing the No U-turn sampler in Stan (Carpenter et al., 2017). Convergence was assessed via visual inspection of traceplots, examination of the R-hat statistic and effective sample size (Gelman & Rubin, 1992). For all models R-hat < 1.01 and effective samples sizes of > 1000 samples were obtained. Typical traceplots for effects $\beta_1 \ldots \beta_3$, random frailty terms ω_1, ω_2 and Weibull shape α are provided in Figure B-1:

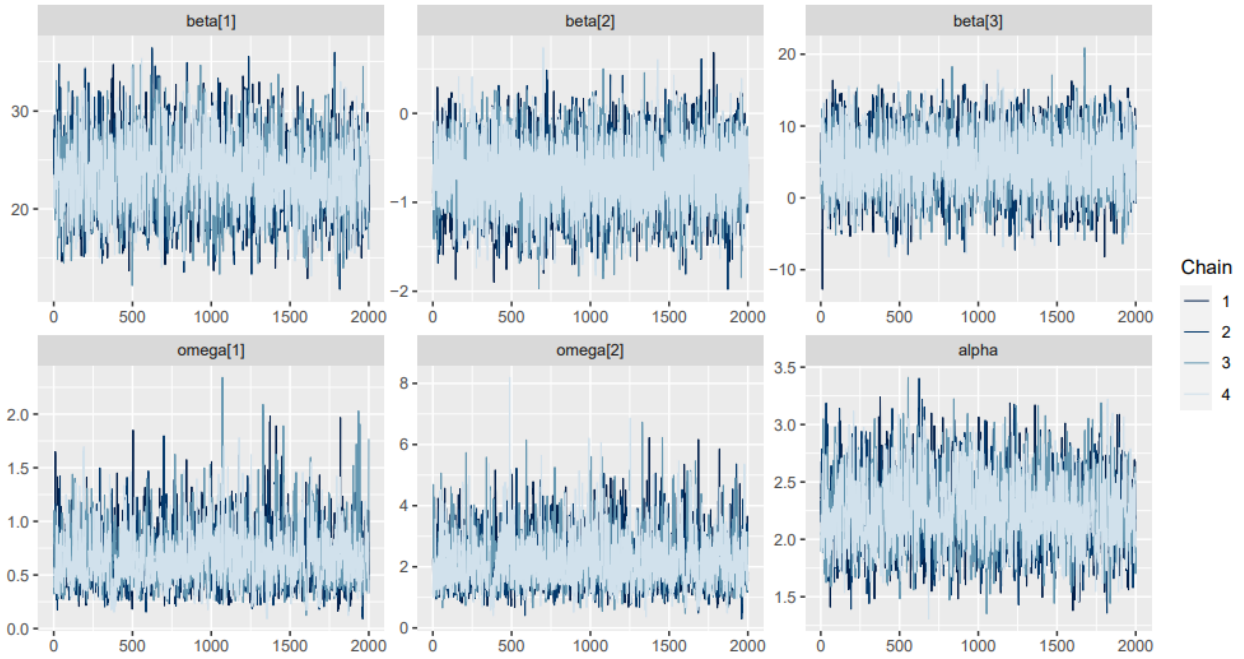

Figure B-1: Typical traceplots for key model parameters

Stan model code is found in Listing B-1.

Listing B-1: Stan Model code for Gamma-Weibull frailty model

```
// Frailty model for Horse fetlock analysis

data {
    int N; // Number of observations
    int<lower=1, upper=N> I; // Number of horses
    int K; // Number of covariates
    array[N] int<lower=1, upper=I> id; // Horse ID
    array[N] int<lower=0,upper=1> status; // Censoring indicatior
    vector[N] y; // Time to event or censoring
    matrix[N, K] X; // Covariates
    real<lower=0> alpha_prior;  // scale of alpha prior
    real<lower=0> psi_prior;  // scale of omega prior
    real<lower=0> beta_prior;  // scale of beta prior
    real<lower=0> mu_prior;     // scale of mu prior
}
transformed data{
    // Center covariates
    matrix[N, K] X_cent = X;
    X_cent[:, 1] = X_cent[:, 1] - mean(X_cent[:, 1]);
    if(K>2){
        X_cent[:, 3] = X_cent[:, 1] .* X_cent[:, 2];
```

```
    }
}


parameters {
    vector[K] beta_raw; // Fixed effects
    vector<lower=0>[I] omega; // Random effects
    real<lower=0> alpha_raw;  // Shape of Weibull
    real<lower=0> psi;
    real mu_raw;
}


transformed parameters {
    vector[N] eta;
    vector[N] sigma;
    real<lower=0> alpha = alpha_prior*alpha_raw;
    real mu = mu_prior*mu_raw;
    //vector[I] omega = omega_prior*omega_raw;
    vector[K] beta = beta_prior*beta_raw;
    for (n in 1:N) {
            eta[n] = X_cent[n, ] * beta;
            sigma[n] = omega[id[n]]*exp(-(mu + eta[n])/alpha);

    }
}

model{

    // Priors
    alpha_raw ~ std_normal();
    omega ~ gamma(psi, psi);
    psi~ gamma(psi_prior, psi_prior);
    beta_raw ~ std_normal();
    mu_raw ~ std_normal();

    // Likelihood
    y ~ weibull(alpha, sigma);

}
```

Appendix C

Using Discrete Element Analysis to Compute Contact Stress in the Equine Metacarpophalangeal Joint

Musculoskeletal injuries are a common cause of lost training time and wastage in racehorses. The metacarpophalangeal (MCP) joint is one of the most commonly affected sites, with fractures of the third metacarpal (MC3) and proximal phalanx (P1) accounting for the majority of fatal bone injuries (Johnson et al., 1994; Rosanowski et al., 2017, 2019). These injuries are believed to be a direct result of the high intensity loading of the skeleton during racing and there is consensus that these injuries represent a mechanical fatigue phenomenon (Martig et al., 2014; Riggs, 1999; Riggs et al., 1999a). While several factors contribute to the development of these fatigue injuries, the magnitude of the stress that the tissue is subjected to plays a critical role. However, the stress experienced by the tissue is challenging to measure *in vivo*. Instead, computational models, such as finite element modelling, are often used to characterize the contact stress within a joint (Harrison et al., 2014; McCarty et al., 2016). However, these models are computationally expensive and time consuming.

Discrete element analysis (DEA) is an alternative computational technique for calculating intra-articular contact stress distributions in a fraction of the time required to obtain the same information using the more commonly employed finite element method. DEA has been applied to the human ankle and has been shown to provide comparable contact stress predictions as the finite element method (Anderson et al., 2010; Townsend et al., 2018), however, it has not yet been applied to the equine MCP joint. Therefore, the purpose of this study was to establish a computational workflow for the estimation of contact stress distributions at the MCP joint using discrete element analysis.

Four distal forelimbs were harvested from four mature horses (3 male and 1 females) euthanized for reasons unrelated to this research. The distal forelimbs were scanned using a Revolution GSI scanner (General Electric Medical System, Milwaukee, WI; acquisition settings: 120 kVp, 200 mA, in-plane resolution of 0.48 × 0.48 mm, slice thickness of 0.625 mm). Bone geometries were segmented in Mimics and exported as stereolithography (STL) files to create triangulated surface meshes for DEA in Matlab (r2021b, Mathworks, MA, USA). STL files were remeshed with a uniform mesh having a target element edge length of 1 mm. DEA was used to estimate contact stress between the MC3 and proximal phalanx P1 and between the MC3 and sesamoids at 11 instances throughout the stance phase of gait. Joint space width between surfaces was calculated in order to adopt an animal-specific, non-uniform cartilage geometry. This was done by constructing vectors as a normal projections from the MC3 subchondral bone surface toward either the P1 or sesamoid subchondral bone surface. Half of the joint space width was taken to be the cartilage thickness at each bone with a modulus of 36 MPa. Applied loads accounted for contributions from tendons, ligaments, and ground reaction forces for a 500 kg horse trotting at a speed of 1.4 m/s (Harrison et al., 2010). From ground contact to midstance, the applied loads ranged from 4000 N to 19,000 N. At this speed, the MCP joint underwent 24° of extension from ground contact to midstance (Clayton et al., 2007). Equilibrium was deemed to have been reached when the net force in each direction was less than 0.1 N. A series of sensitivity analyses were conducted to investigate the influence of cartilage thickness, cartilage stiffness, and loading magnitude on the resulting contact stress distribution.

All four cases had a mean (SD) cartilage thickness of 0.94 (0.06) mm (Figure C-1).

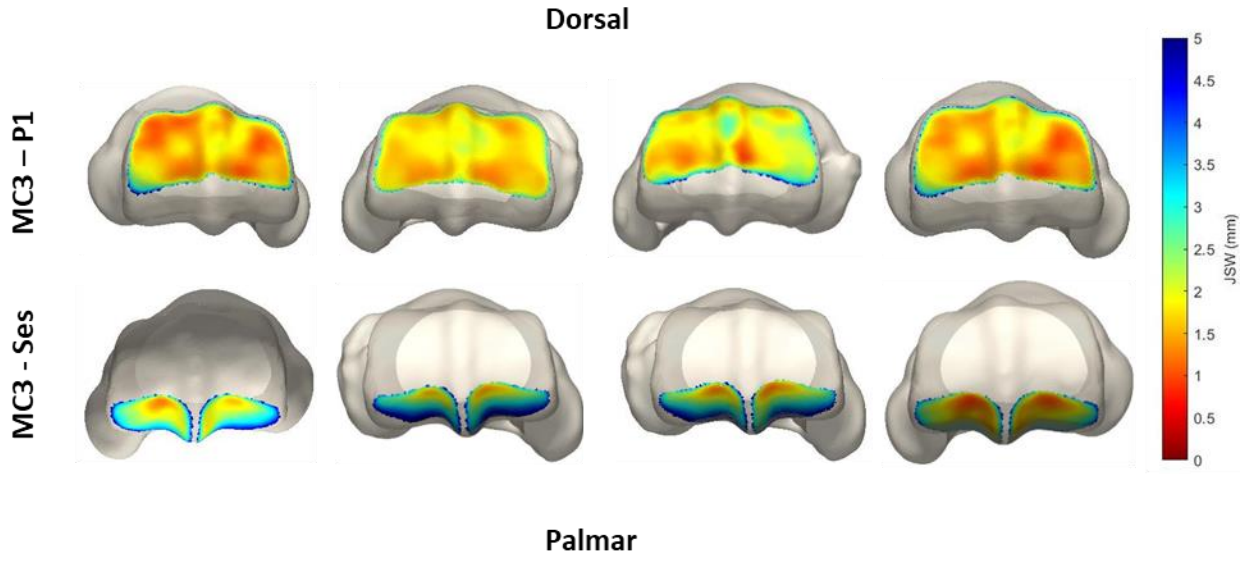

Figure C-1: Joint space width measurement between the (top) MC3 and P1, and (bottom) MC3 and sesamoids for four different limbs

Mean and peak contact stress distributions are summarized in Table C-1. The contact stress distributions are represented in Figure C-2.

Table C-1: Peak and mean contact stress within the MCP joint from the DEA

Joint Contact	**Peak Stress (SD) MPa**	**Mean Stress (SD) MPa**
MC3 – P1	83 (21)	25 (3)
MC3 – Ses	121(46)	35 (4)

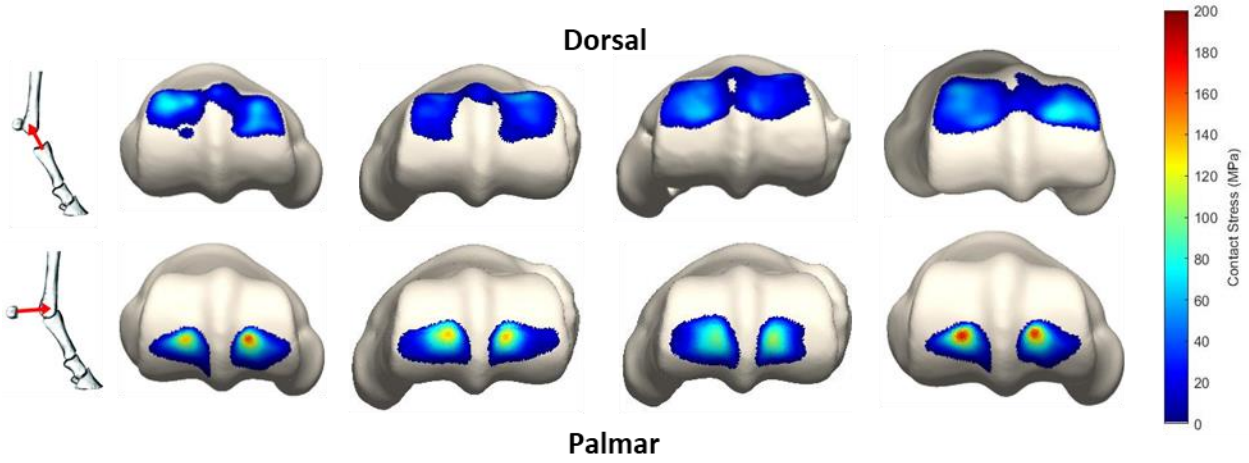

Figure C-2: Contact stress distribution between the (top) MC3 and P1, and (bottom) MC3 and sesamoids for four different limbs

The results of the sensitivity analysis investigating the influence of cartilage stiffness, cartilage thickness, applied load, and a uniform cartilage distribution on the resulting contact stress distribution are summarized in Table C-2.

Table C-2: Results from the sensitivity analysis investigating the influence of model parameters on the resulting contact stress distribution

	10% Increase in Cartilage Stiffness	10% Increase in Cartilage Thickness	10% Increase in Applied Load	Uniform Cartilage Thickness
Change in Peak Stress	+ 5.3%	- 4.9%	+ 4.6%	- 26.7%
Change in Mean Stress	+ 4.7%	- 4.8%	+ 4.7%	- 12.4%
Change in Contact Area	- 4.7%	+ 5.4%	+ 5.4%	+ 14.9%

The mean cartilage thickness values reported from this model (0.94 mm) are consistent with *in vivo* measurement of cartilage thickness at the MCP joint (0.86 mm) (Lee et al., 2014). To verify the discrete element model, results were compared against an existing finite element model (Harrison et al., 2014). DEA reported comparable contact stresses to the FEA model (Table C-3).

Table C-3: Comparing peak and mean stress from the DEA with an existing finite element model (Harrison et al., 2014)

Joint Contact	Peak Stress (SD) MPa		Mean Stress (SD) MPa	
	DEA	FEA	DEA	FEA
MC3 – P1	83 (21)	110	25 (3)	25
MC3 – Ses	121 (46)	99	35 (4)	32

The calculations of joint contact pressure from this DEA are comparable to those reported from an existing finite element model, suggesting that DEA can be used to effectively estimate contact stress distribution at the MCP joint. Although cartilage stiffness and thickness assumptions influenced DEA predicted outcomes, changes to peak stress magnitudes were only moderately sensitive to these assumptions. What gives us further confidence in this model is the locations where the peak stresses were seen. Higher stresses were experienced between the MC3-sesamoid contact and peak stresses were seen at the palmar aspect of the MC3. This is a location where tendon wrapping generates extreme cyclical loads between the sesamoid bones and the MC3 during high-speed training and racing (Harrison et al., 2010; Merritt et al., 2008). Although similar joint contact forces are experienced between the MC3-P1 joint and the MC3-sesamoid contact, the higher contact stress at the MC3-sesamoid joint is likely due to the loads being distributed over a smaller contact area. Peak stresses were also consistently clustered near the condylar grooves of the MC3, which is where many condylar fractures originate (Riggs, 1999; Riggs et al., 1999a).

Therefore, the model-predicted distributions of contact stress are consistent with the locations of joint surface injury commonly observed in the distal equine forelimb. This work demonstrated that DEA is an efficient method to accurately determine the contact stress in the MCP joint and may help us better understand the fatigue limits of subchondral bone and provide some insight into the development of these injuries.